A well-balanced all-Mach scheme for compressible two-phase flow

Computer Physics Communications 299 (2024) 109131

Contents lists available at ScienceDirect

Computer Physics Communications

journal homepage: www.elsevier.com/locate/cpc

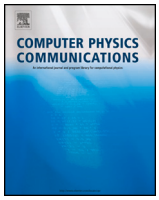

Computational Physics

A well-balanced all-Mach scheme for compressible two-phase flow ☆

Sandro Malusà [a,b,*,1], Alessandro Alaia [a]

[a] Optimad Engineering, Via Agostino da Montefeltro, 2, Turin, 10134, Italy
[b] Politecnico di Torino, Corso Duca degli Abruzzi, 24, Turin, 10129, Italy

ARTICLE INFO

Keywords:
Compressible two-phase flow
Two-phase flow
All-Mach scheme
IMEX-RK scheme
Well-balanced scheme
Asymptotic-preserving

ABSTRACT

We present an implicit-explicit finite volume scheme for the compressible two-phase model in all-Mach number regimes. In order to solve model equations efficiently and accurately in the low Mach regime, the convective term is split in a stiff part associated to fast acoustic waves, and a non-stiff part corresponding to mean flow advection. A Implicit-Explicit Runge-Kutta (IMEX-RK) method is used to integrate the stiff part implicitly, while non-stiff terms are treated explicitly. This leads to a predictor-corrector scheme, where the contribution of pressure waves is accounted for by solving a system of non-linear elliptic equations for the phasic pressures. The resulting numerical scheme is well-balanced and stable under a CFL condition based on the macroscopic velocity only and is capable of simulating two-phase flows in both the incompressible limit and in the highly compressible regime. The asymptotic preserving property of the scheme is also proven.

1. Introduction

Two-phase flows are encountered in a wide range of scenarios both in nature and industrial processes. Some examples of natural flows include sedimentation and groundwater flows. In industrial applications, two-phase flows are encountered in fluidized bed, nuclear reactors, pipelines for crude oil transport, micro-mixers for drug synthesis, and trickle bed reactors in chemical industry, just to name a few. Depending on the flow rate of each phase, different types of regimes can be observed, ranging from dispersed bubbly flow to separated stratified flow. Such a variability poses an intrinsic challenge in modeling. Even for the simplest cases, there is not an uniquely accepted formulation of the governing equations.

Our target application is the numerical simulation of Trickle Bed Reactors (TBR) for biological methanation. This is a relatively new application which is gaining momentum due to the increasing demand of energy from renewable sources [1]. In TBRs for biological methanation, renewable hydrogen and carbon dioxide are converted into methane as the result of the biological Sabatier reaction happening inside microorganisms of the Archaea family. Gaseous reactants are introduced inside a reactor together with an aqueous phase (either co-currently or counter-currently). Hydrogen and carbon dioxide dissolve in the liquid phase and are harvested by microorganisms living on the surface of a packed bed. After the Sabatier reaction takes place, methane is released as a gaseous phase. Performances of these reactors are measured in terms of production rate and degree of purity of methane, and are heavily influenced by operating conditions (temperature and pressure), and by the *wetting efficiency*. The latter is related to the percentage of solid surface covered by the liquid phase. Therefore, accurate simulations of hydrodynamics in TBRs are of paramount importance during the design phase and for scale-up.

From the computational point of view, the main challenges are related to the accurate simulation of the *trickle regime*, which is characterized by strong inhomogeneities of phase distribution and complex geometry of the interface between phases. As a consequence, direct numerical simulations and interface tracking methods would require prohibitive grid resolutions and computational times not compatible with industrial turn-overs. Furthermore, due to volume variations resulting from the heterogeneous Sabatier reaction, incompressible solvers cannot be readily used. Instead, one has to resort to compressible solvers, where the main challenge is the efficient and accurate simulation of the slow flow dynamics. For such reasons, the use of all-Mach numerical schemes appears compelling, as these methods are capable of maintaining a good accuracy in the incompressible limit and do not suffer from time step restrictions typical of explicit solvers.

☆ The review of this paper was arranged by Prof. David W. Walker.

* Corresponding author at: Politecnico di Torino, Corso Duca degli Abruzzi, 24, Turin, 10129, Italy.
E-mail addresses: sandro.malusa@optimad.it (S. Malusà), alessandro.alaia@optimad.it (A. Alaia).

[1] This is the first author.

https://doi.org/10.1016/j.cpc.2024.109131
Received 25 August 2023; Received in revised form 19 January 2024; Accepted 12 February 2024
Available online 15 February 2024

Most of the model equations available in the literature for compressible multiphase flows refer to the Baer-Nunziato model [2], where each phase has a different velocity and is governed by its own equation of state (EOS). In order to derive the governing equations for the Baer-Nunziato model, volume averaging is applied to single-phase conservation laws using the procedure described in [3]. The resulting averaged equations describe balance laws for mass, momentum and energy of each phase, and include coupling terms for interphase friction forces, and pressure relaxation terms. The latter describe the relaxation of each phase towards a thermodynamic equilibrium shared among all phases. Simpler models can be derived from Baer-Nunziato equations under the assumption that all phases share the same velocity (*six equations* models, see [4], [5], [6]), the same pressure and velocity (*five equations* models, see [7], [8], [9], [10], [11], [12]) or the same pressure, velocity and temperature (*four equations* models, see [13]). Another class of six-equations models is based on the assumption that all phases share the same pressure but have separate velocities. These models are known to be ill-posed as discussed in [14].

Our ultimate goal is the numerical simulation of a TBR for biological methanation including dissolution processes and chemical reactions. However, in the present work, we focus solely on the development of an all-Mach scheme for compressible two-phase flows. This represents the very first step towards *efficient* numerical simulations of TBRs.

The design of an efficient all-Mach numerical schemes is still an active area of research, with most of the research effort focusing on single-phase flows. The basic idea behind an all-Mach numerical scheme is to resolve acoustic perturbations implicitly, while an explicit method is used to integrate model equations for the mean flow (see for instance, [15], [16], [17], [18] and [19]). The advantage of such a strategy is two-fold. On one hand, the time step restriction due to the fast-traveling acoustic waves is avoided rendering the numerical solution of these equations efficient in the low-Mach regime. On the other hand, the simplicity and robustness of explicit methods is retained in the compressible regime. This idea has been extended to two-phase flows in [20] for the isentropic case and in [21]. However, to our knowledge, this is one of the first attempts to apply the all-Mach philosophy to the complete Baer-Nunziato model.

Our numerical scheme is based on the well-known Implicit-Explicit (IMEX) Runge-Kutta (RK) time integration scheme [22], which is used to integrate implicitly the stiff part of the convective term, while the non-stiff part of the convective term is treated explicitly. Although the structure of conservative terms allows to re-use much of the well-established numerical methods for conservation laws, proper discretization of non-conservative terms is required to obtain a well-balanced scheme, that is a numerical scheme capable of preserving steady states also at the discrete level. Furthermore, special care is required for the numerical treatment of pressure coupling terms, as discussed in [23]. The well-balancing strategy proposed in this work is novel to the best of our knowledge and generalizes the idea of Abgrall and Saurel in the framework of an IMEX-RK numerical scheme. The balancing procedure results in a non-trivial discretization of the volume fraction equation.

Even though in our target application both phases are in the same Mach regime, our numerical scheme generalizes well also to the less common cases where a phase is approaching the low Mach limit and the other is in the compressible regime. In this regard, we propose a proof of the asymptotic preserving property valid for both cases.

The reminder of this paper is organized as follows. In section 2, model equations for compressible two-phase flows are presented. Non-dimensional analysis is carried out in section 2.2 to identify stiff and non-stiff terms while in section 2.3 the low-Mach limit of the system and well-prepared initial data are derived. In section 3, we introduce the IMEX-RK semi-discrete scheme and we derive a non-linear elliptic equation for the implicit pressure step. In section 4 we present the fully discrete scheme and introduce the balancing procedure. In section 5, we prove that our numerical scheme is Asymptotic Preserving (AP) in the sense introduced in [24], and discussed in [25] and [19]. Lastly, in section 6, we present several numerical experiments which demonstrate the capability of our scheme to accurately simulate two-phase flows both in the compressible regime and in the incompressible limit.

2. Model equations

2.1. Compressible two-phase flow model

Our model equations are the volume averaged equations for compressible two-phase flows as derived by Abgrall and Saurel in [23]. Details on the averaging procedure can be found in [26] and [3].

For the one-dimensional case, the equations read as follows:

$$\begin{aligned}
\partial_t \alpha_k + u_I \partial_x \alpha_k &= \sum_{j\neq k} \nu_{k,j}(p_k - p_j) \\
\partial_t(\alpha_k \rho_k) + \partial_x\left(\alpha_k \rho_k u_k\right) &= 0 \\
\partial_t(\alpha_k \rho_k u_k) + \partial_x\left(\alpha_k \rho_k u_k^2 + \alpha_k p_k\right) &= p_I \partial_x \alpha_k + \sum_{j\neq k} F_{k,j} \\
\partial_t(\alpha_k \rho_k E_k) + \partial_x\left(u_k\left(\alpha_k \rho_k K_k + \alpha_k \rho_k H_k\right)\right) &= p_I u_I \partial_x \alpha_k + u_I \sum_{j\neq k} F_{k,j} \\
&\quad - \sum_{j\neq k} \nu_{k,j} p_I (p_k - p_j)
\end{aligned} \tag{1}$$

where $(t,x) \in [0,T] \times \Omega$, Ω is the computational domain and T is the final integration time. Subscript $k = 1,2$ is the phase index, and I is used for quantities evaluated at the material interface.

As mentioned in the introduction, the focus of this work is on the derivation of an all-Mach numerical scheme for two-phase flows. Therefore in the above equations, we omit terms accounting for dissolution processes and heterogeneous chemical reactions which would appear as source terms in mass, momentum and energy equations. Furthermore, we omit terms related to viscous forces in the bulk of each phase, namely the stress tensor and the deviatoric stress tensor. While these terms play a significant role in the simulation of TBR hydrodynamics, from a numerical point of view they do not pose a significant challenge and standard numerical techniques can be used to discretize these terms.

The first eq. in (1) describes advection of volumetric fractions (α_k) with interface velocity u_I. Volumetric fractions obey the compatibility condition $\sum_k \alpha_k = 1$. The l.h.s. of the remaining equations describe balance laws for mass, momentum and energy of each individual phase weighted by the volumetric fraction. Notation is standard. ρ_k, u_k, p_k, represent density, velocity, pressure for phase k averaged over a reference volume centered at (x,t). Specific kinetic energy, total energy, and total enthalpy are related to primitive variables as follows:

$$K_k = \frac{1}{2}u_k^2, \qquad E_k = e_k + K_k, \qquad H_k = e_k + \frac{p_k}{\rho_k} \tag{2}$$

where e_k is the (specific) internal energy and is related to pressure and density by the equation of state $p_k = p_k(e_k, \rho_k)$. Although our derivation can be generalized to more complex equations of state, in this paper we consider the following EOS:

$$\text{Perfect gas:} \qquad \rho e = \frac{p}{\gamma - 1} \tag{3a}$$

$$\text{Stiffened EOS:} \qquad \rho e = \frac{p + \gamma p_\infty}{\gamma - 1} = \frac{p}{\beta} + \frac{\eta}{\beta}. \tag{3b}$$

On the r.h.s. of equations (1), $F_{k,j}$ represents the drag force acting at the interface between phases k and j. Non-conservative term $p_I \partial_x \alpha_k$ (and its counterpart in the energy equation) models the force (work) resulting from spatial variations of the volumetric fraction. Lastly, term $\nu_{k,j}(p_k - p_j)$ is introduced to account for thermodynamic (pressure) relaxation for the pair of phases (k,j) at rate $\nu_{k,j}$.

To avoid spurious contributions to total energy and momentum, the following compatibility conditions must hold:

$$\sum_k p_I \partial_x \alpha_k + \sum_{j\neq k} F_{k,j} = 0$$
$$\sum_k p_I u_I \partial_x \alpha_k + u_I \sum_{j\neq k} F_{k,j} - \sum_{j\neq k} v_{k,j} p_I (p_k - p_j) = 0 \tag{4}$$
$$F_{k,j} = -F_{j,k}$$

which describe force equilibrium and the energy conservation across the interface between phase k and j.

In order to close the above system of equations, relationships for drag forces and relaxation rates must be specified. Closure relationships strongly depend on the test case and regime under consideration. Without loss of generality, we assume that the drag force is proportional to the relative velocity between two phases, that is:

$$F_{k,j} = \tau_{k,j}(u_k - u_j),$$

where $\tau_{k,j}$ represents the rate at which both velocities are homogenized towards a common value. Other examples of interfacial drag forces are available in [27] and references therein.

Similarly, a closure relationship for the pressure relaxation rate, $v_{k,j}$, must be provided. In this work, we assume that pressure relaxation is instantaneous (as in [23]), which corresponds to the case of thermodynamic processes happening on a time scale much smaller than the characteristic convective time. This is approximately true for slow flows characterized by weak pressure imbalances between phases. However, more general relaxation models can be incorporated in our numerical scheme.

Finally, p_I and u_I represent the average pressure and velocity at the interface between phases. In this paper, we adopt the common choice of setting:

$$p_I = \sum_k \alpha_k p_k, \qquad u_I = \frac{\sum_k \alpha_k \rho_k u_k}{\sum_k \alpha_k \rho_k}. \tag{5}$$

Knowing conservative and primitive quantities for each phase, mixture density, velocity and pressure can be expressed as follows:

$$\rho = \sum_k \alpha_k \rho_k, \qquad u = \frac{1}{\rho}\sum_k \alpha_k \rho_k u_k, \qquad p = \sum_k \alpha_k p_k \tag{6}$$

It is easy to show that the system of equations (1) is hyperbolic with eigenvalues for phase k given by:

$$\lambda_I = u_I,$$
$$\lambda_k^+ = u_k + c_k, \quad \lambda_k^0 = u_k, \quad \lambda_k^- = u_k - c_k, \tag{7}$$

where c_k is the speed of sound and can be computed as follows:

$$c_k^2 = \frac{\frac{p_k}{\rho_k^2} - \left.\frac{\partial e_k}{\partial \rho_k}\right|_{p_k}}{\left.\frac{\partial e_k}{\partial p_k}\right|_{\rho_k}} \tag{8}$$

$\lambda_k^{\pm}$ are the eigenvalues associated to (fast) acoustic waves, λ_k^0 is the eigenvalue associated to the mean flow velocity and λ_I is the eigenvalue corresponding to the interface velocity, that is the velocity at which the material interface is advected throughout the domain.

For a standard explicit time integration method, the CFL condition is given by:

$$\Delta t \leq C\,\frac{\Delta x}{\lambda_{\max}} \leq \frac{C\,\Delta x}{\max_{k,\Omega}(|u_k| + c_k)} \leq \frac{C \min_{k,\Omega}(M_k)\Delta x}{\max_{k,\Omega}(|u_k|(M_k+1))} \tag{9}$$

where $M_k = u_k/c_k$ and $C \leq 1$ is the Courant number. Note that the maximum time step allowed is governed by the Mach number of the least compressible phase and becomes computationally prohibitive when simulating flows characterized by slow dynamics.

2.2. Non-dimensional equations

The starting point for the derivation of the all-Mach scheme is the non-dimensional form for equations (1). To this end, we assume that material velocities and pressures for each phase are roughly in the same order of magnitude. This assumption holds true for flows characterized by slow dynamics as those encountered in TBRs.

Let $u^r = x^r/t^r$ and p^r be the reference velocity and pressure, where x^r and t^r are a reference length and time scales. Even though we assume similar pressures and velocities for both phases, it is necessary to allow for big differences in densities (as it happens, for instance, in gas-liquid mixtures). To this end, we denote the reference mixture density by ρ^r and the reference phase densities as $\rho_1^r = \varrho_1\rho^r$, $\rho_2^r = \varrho_2\rho^r$ as done in [20], where $\varrho_1, \varrho_2 \in \mathbb{R}$ are scaling constants. Using the above reference quantities, the reference speeds of sound and Mach number for phase $k = 1, 2$ are given by:

$$(c_k^r)^2 = \frac{p^r}{\varrho_k \rho^r}, \qquad M_k^r = \frac{u^r}{c_k^r}. \tag{10}$$

The resulting non-dimensional quantities denoted by $\tilde{\cdot}$ are:

$$\begin{aligned}
\rho_k &= \tilde{\rho}_k \varrho_k \rho^r, \qquad \rho = \rho^r \sum_k \alpha_k \tilde{\rho}_k \varrho_k = \tilde{\rho}\rho^r,\\
u_k &= \tilde{u}_k u^r, \qquad u_I = u^r \frac{\sum_k \alpha_k \tilde{\rho}_k \varrho_k \tilde{u}_k}{\tilde{\rho}},\\
p_k &= \tilde{p}_k p^r, \qquad p_I = p^r \sum_k \alpha_k \tilde{p}_k\\
e_k &= \tilde{e}_k \frac{p^r}{\rho_k^r}, \qquad \tilde{E}_k = \tilde{e}_k + \frac{1}{2} M_k^2 \tilde{u}_k^2
\end{aligned} \tag{11}$$

Finally, we write the non-dimensional relaxation rate, $v_{k,j}$, as:

$$\tilde{v}_{k,j} = \frac{v_{k,j}}{t^r \rho^r u^r u^r}. \tag{12}$$

Adimensionalization of (1) yields to the following system of equations:

$$\begin{aligned}
&\partial_t \alpha_k + u_I \partial_x \alpha_k = \sum_{j\neq k} v_{k,j}\left(\frac{\varrho_k p_k}{M_k^2} - \frac{\varrho_j p_j}{M_j^2}\right)\\
&\partial_t(\alpha_k \rho_k) + \partial_x\left(\alpha_k \rho_k u_k\right) = 0\\
&\partial_t(\alpha_k \rho_k u_k) + \partial_x\left(\alpha_k \rho_k u_k u_k + \frac{\alpha_k p_k}{M_k^{r2}}\right) = \frac{p_I}{M_k^{r2}}\partial_x \alpha_k + \sum_{j\neq k} F_{k,j}\\
&\partial_t(\alpha_k \rho_k (e_k + M_k^{r2} K_k)) + \partial_x\left(u_k\left(M_k^{r2}\alpha_k \rho_k K_k + \alpha_k \rho_k H_k\right)\right) = p_I u_I \partial_x \alpha_k\\
&+ M_k^{r2} u_I \sum_{j\neq k} F_{k,j} - \sum_{j\neq k} v_{k,j} p_I \left(\frac{\varrho_k p_k}{M_k^2} - \frac{\varrho_j p_j}{M_j^2}\right)
\end{aligned} \tag{13}$$

where $\tilde{\cdot}$ has been omitted for clarity and $k, j = 1, 2$.

The above adimensional equations show that pressure terms in the momentum equation scale with $1/M_k^{r2}$. Moreover in the energy equation, time derivative of internal energy, space derivatives of total enthalpy, the interface pressure scale and pressure relaxation terms all scale as $1/M_k^{r2}$. These terms represent the stiff part of our model equations in the low Mach limit.

2.3. Low Mach limit and well-prepared initial data

In this section we derive the limiting equations for the Baer-Nunziato model in the low-Mach number limit. We focus our analysis on the following cases:

- **Case 1:** All phases are approaching the (low) Mach regime simultaneously ($M_1 = M_2 = M$).
- **Case 2:** One phase is compressible ($M_1 = 1$), while the other is approaching the low Mach limit ($M_2 \ll 1$).

Case 1 Let both phases be in the same Mach regime, i.e. $M_1 \approx M_2$. We expand primitive variables, with respect to the common Mach number M as follows:

$$\begin{aligned}
\rho_k &= \rho_{k,0} + M\rho_{k,1} + M^2\rho_{k,2},\\
u_k &= u_{k,0} + Mu_{k,1} + M^2u_{k,2},\\
p_k &= p_{k,0} + Mp_{k,1} + M^2p_{k,2},\\
u_I &= u_{I,0} + Mu_{I,1} + M^2u_{I,2},\\
p_I &= p_{I,0} + Mp_{I,1} + M^2p_{I,2},
\end{aligned}$$

and we assume $\alpha_k = \alpha_{k,0} + O(M)$. Note that when both Mach numbers are in the same order, we have:

$$M_1^2 = \frac{\rho^r\varrho_1 u^r u^r}{p^r} = \frac{\rho^r\varrho_2 u^r u^r}{p^r} = M_2^2 \quad \Longrightarrow \quad \varrho_1 = \varrho_2. \tag{14}$$

Substituting the above expansions in the volume fraction equation, we immediately obtain:

$$\begin{aligned}
O(1/M^2) \quad & p_{1,0} = p_{2,0} = p_0\\
O(1/M) \quad & p_{1,1} = p_{2,1} = p_1
\end{aligned} \tag{15}$$

and at order $O(1)$:

$$\partial_t\alpha_{k,0} + u_{I,0}\partial_x\alpha_{k,0} = \nu_{k,j}(\varrho_k p_{k,2} - \varrho_j p_{j,2}), \quad k,j = 1,2,\ k \neq j. \tag{16}$$

Next, we substitute variable expansions in the momentum equation. We obtain (order $O(1/M^2)$):

$$\partial_x(\alpha_{k,0}p_0) = p_{I,0}\partial_x\alpha_{k,0} \qquad k = 1,2 \tag{17}$$

and (order $O(1/M)$):

$$\partial_x(\alpha_{k,0}p_1) = p_{I,1}\partial_x\alpha_{k,0} \qquad k = 1,2. \tag{18}$$

By adding eqs. (17) written for both phases, we obtain:

$$\partial_x(p_0(\alpha_{1,0} + \alpha_{2,0})) = p_{I,0}\partial_x(\alpha_{1,0} + \alpha_{2,0})$$

Next, we assume that $\alpha_{1,0} + \alpha_{2,0} = 1$, from which we immediately deduce:

$$\partial_x p_0 = 0.$$

Similarly, we obtain that $\partial_x p_1 = 0$ from terms at order $O(1/M)$.

If instead we subtract eqs. (17) written for each phase, we obtain:

$$\partial_x(p_0(\alpha_{1,0} - \alpha_{2,0})) = p_{I,0}\partial_x(\alpha_{1,0} - \alpha_{2,0})$$

Using the fact that $\partial_x p_0 = 0$, we get $p_0 = p_{I,0}$. Analogously, from term at order $O(1/M)$, we obtain $p_1 = p_{I,1}$.

The full system at order $O(1)$ reads:

$$\begin{cases}
\partial_t(\alpha_{k,0}\rho_{k,0}) + \partial_x\left(\alpha_{k,0}\rho_{k,0}u_{k,0}\right) & = 0\\
\partial_t(\alpha_{k,0}\rho_{k,0}u_{k,0}) + \partial_x\left(\alpha_{k,0}\rho_{k,0}u_{I,0}u_{I,0} + \alpha_{k,0}p_{k,2}\right) & = p_{I,2}\partial_x\alpha_{k,0} + \sum_{k\neq j} F_{k,j}\\
\partial_t(\alpha_{k,0}\rho_{k,0}e_{k,0}) + \partial_x\left(u_{k,0}(\alpha_{k,0}\rho_{k,0}e_{k,0} + \alpha_{k,0}p_0)\right) & = p_0u_{I,0}\partial_x\alpha_{k,0}\\
& \quad -\nu_{k,j}p_0(\varrho_k p_{k,2} - \varrho_j p_{j,2})\\
\partial_t\alpha_{k,0} + u_{I,0}\partial_x\alpha_{k,0} & = \nu_{k,j}(\varrho_k p_{k,2} - \varrho_j p_{j,2}),
\end{cases} \tag{19}$$

which suggests that when both phases are in the same Mach regime, pressure perturbations are second order effects and are due to pressure imbalances across the material interface. Therefore, we can write:

$$p_k(x,t) = p(t) + M^2p_{k,2}(x,t) \quad k = 1,2 \tag{20}$$

$$p_I(x,t) = p(t) + M^2p_{I,2}(x,t) \tag{21}$$

where $p = p(t)$ changes in time only due to boundary conditions.

From now on, we assume that both phases are governed by the equation of state for perfect gasses:

$$p_k = (\gamma - 1)\rho_k e_k$$

The expansion for internal energy is:

$$e_k = \frac{p_0}{\rho_{k,0}} + M\left(\frac{p_1}{\beta_k\rho_{k,0}} + \frac{p_{k,2}}{\beta_k\rho_{k,1}}\right) + O(M^2). \tag{22}$$

Assuming for simplicity that boundary conditions are constant in time and that $u_{k,0} = u_{I,0} = u_0$, we obtain from energy equation in (19):

$$p_0\partial_t\alpha_{k,0} + p_0\partial_x(\alpha_{k,0}u_0 + \alpha_{k,0}u_0) = p_0u_0\partial_x\alpha_{k,0} - \nu_{k,j}p_0(\varrho_k p_{k,2} - \varrho_j p_{j,2}) \tag{23}$$

Subtracting the volumetric fraction equation in (19) multiplied by p_0, we obtain:

$$\alpha_{k,0}\partial_x(u_0) = -\nu_{k,j}(\varrho_k p_{k,2} - \varrho_j p_{j,2}). \tag{24}$$

From eq. (24), we note that in the bulk of the fluid $\partial_x u_0 = 0$, since the relaxation term on the right hand side vanishes. Instead, at the material interface, we have that $\partial_x u_0 \neq 0$ since in general pressure across the material interface might be different.

This is coherent with the physical behavior of the system. When an acoustic wave propagates across the material interface, pressure relaxation triggers a volume variation in each phase (see volumetric fraction equation) to compensate for the pressure imbalance between phases. In most practical situations however, pressure relaxation is faster than advection phenomena. Thus, we can assume an instantaneous pressure relaxation which leads to $p_{k,2} = p_{j,2}$ and the incompressibility condition is recovered also at the material interface.

It is worth noticing that in the one-dimensional setting, the above derivation implies that the leading term of the velocity field is constant in space. Instead, in higher spatial dimensions, it leads to a divergence-free velocity field.

To summarize, the set of model equations in the limit $M \to 0$ (assuming instantaneous pressure relaxation) is:

$$\begin{cases}
\partial_t(\alpha_{k,0}\rho_{k,0}) + u_0\partial_x\left(\alpha_{k,0}\rho_{k,0}\right) = 0\\
\partial_t(\alpha_{k,0}\rho_{k,0}u_0) + u_0\partial_x\left(\alpha_{k,0}\rho_{k,0}u_0\right) + \partial_x(\alpha_{k,0}p_{k,2}) = p_{I,2}\partial_x\alpha_{k,0} + \sum_{k\neq j} F_{k,j}\\
\partial_t\alpha_{k,0} + u_0\partial_x\alpha_{k,0} = 0\\
\partial_x u_0 = 0
\end{cases} \tag{25}$$

and the well-prepared initial data is given by:

$$\Psi_M^{wp} = \Big\{\psi \in \mathbb{R}^{2d+3} : p_{k,0} = p_0,\ p_{k,1} = p_1,\ u_{k,0} = u_{I,0} = u_0, \quad \partial_x u_0 = 0,\ \text{for } k = 1,2\Big\} \tag{26}$$

Case 2 We now consider the case when one phase is compressible ($M_1 = 1$) while the other is approaching the low Mach limit $M_2 \to 0$.

Primitive variables for the phase approaching the low Mach limit are expanded as follows:

$$\begin{aligned}
\rho_2 &= \rho_{2,0} + M_2\rho_{2,1} + M_2^2\rho_{2,2},\\
u_2 &= u_{2,0} + M_2u_{2,1} + M_2^2u_{2,2},\\
p_2 &= p_{2,0} + M_2p_{2,1} + M_2^2p_{2,2},\\
\alpha_2 &= \alpha_{2,0} + M_2\alpha_{2,1} + M_2^2\alpha_{2,2},\\
u_I &= u_{I,0} + M_2u_{I,1} + M_2^2u_{I,2},
\end{aligned} \tag{27}$$

while primitive variables for the other phase are set as follows:

$$\begin{aligned}
\rho_1 &= \rho_{1,0} + O(M_2),\\
u_1 &= u_{1,0} + O(M_2),\\
p_1 &= p_{1,0} + O(M_2),\\
\alpha_1 &= \alpha_{1,0} + M_2\alpha_{1,1} + M_2^2\alpha_{1,2}.
\end{aligned} \tag{28}$$

Given that $p_I = \alpha_1 p_1 + \alpha_2 p_2$, the interface pressure, p_I, can be expanded in turn as:

$$p_I = \alpha_{1,0}p_{1,0} + \alpha_{2,0}p_{2,0} + M_2(\alpha_{2,0}p_{2,1} + \alpha_{2,1}p_{2,0} + \alpha_{1,1}p_{1,0}) + M_2^2(\alpha_{2,0}p_{2,2} + \alpha_{2,2}p_{2,0} + \alpha_{2,1}p_{2,1} + \alpha_{1,2}p_{1,0}) = p_{I,0} + M_2 p_{I,1} + M_2^2 p_{I,2}. \tag{29}$$

Inserting variable expansions in the volumetric fraction equation for phase k, we obtain:

$$\begin{aligned} &O(1/M_2^2) \quad p_{2,0} = 0 \\ &O(1/M_2) \quad p_{2,1} = 0 \end{aligned} \tag{30}$$

while at the 0^{th} order for phase 2 we have:

$$\partial_t \alpha_{2,0} + u_{I,0}\partial_x \alpha_{2,0} = \nu_{2,1}(\varrho_2 p_{2,2} - \varrho_1 p_{1,0}) \tag{31}$$

and for phase 1:

$$\partial_t \alpha_{1,0} + u_{I,0}\partial_x \alpha_{1,0} = \nu_{1,2}(\varrho_1 p_{1,0} - \varrho_2 p_{2,2}) \tag{32}$$

From the above relationships, it follows that $p_2 = p_{2,2}M_2^2$. We now substitute variable expansions in the momentum equation of phase 2. By using the above results, we obtain:

$$\begin{aligned} &O(1/M_2^2) \quad : \quad 0 = \partial_x(\alpha_{2,0}p_{2,0}) = p_{I,0}\partial_x \alpha_{2,0} \\ &O(1/M_2) \quad : \quad 0 = \partial_x(\alpha_{2,0}p_{2,1} + \alpha_{2,1}p_{2,0}) = p_{I,1}\partial_x \alpha_{2,0} + p_{I,0}\partial_x \alpha_{2,1} \end{aligned} \tag{33}$$

where we have $p_{I,0} = \alpha_{1,0}p_{1,0}$. In domain regions where only one phase is present, we retrieve the single phase Euler equations for which the asymptotic limit is well known. So we focus on those regions where both phases are simultaneously present, i.e. $\alpha_{1,0} \neq 0$. Furthermore, we assume $p_{1,0}(x,t) \neq 0$, so that eqs. (33) give $\partial_x \alpha_{2,0} = 0$ and $\partial_x \alpha_{2,1} = 0$.

Energy equation for the weakly compressible phase at order 0, can be written as follows:

$$\partial_t(\alpha_{2,0}\rho_{2,0}e_{2,0}) + \alpha_{2,0}\partial_x(u_{2,0}\rho_{2,0}e_{2,0}) = -\nu_{2,1}p_{I,0}(\varrho_2 p_{2,2} - \varrho_1 p_{1,0}). \tag{34}$$

From the previous equations, we have that $p_{2,0} = 0$, which means that at the 0^{th} order the state of the weakly compressible phase is formally a near-vacuum state. For an ideal gas law this would lead to $\rho_{2,0} = 0$. Since we are interested in regions containing both phases, we assume the stiffened gas EOS for phase 2. By replacing the expanded variables, we obtain the expansion for the internal energy:

$$e_2 = \frac{\eta_2}{\beta_2 \rho_{2,0}} + O(M_2). \tag{35}$$

We can now substitute this expansion in eq. (34) to obtain:

$$\frac{\eta_2}{\beta_2}\partial_t(\alpha_{2,0}) + \frac{\alpha_{2,0}\eta_2}{\beta_2}\partial_x(u_{2,0}) = -\nu_{2,1}p_{I,0}(\varrho_2 p_{2,2} - \varrho_1 p_{1,0}) \tag{36}$$

Next we add the $O(1)$ terms of the volume fraction equation (31) for phase 2 multiplied by $p_{I,0}$ which gives:

$$\left(\frac{\eta_2}{\beta_2} + p_{I,0}\right)\partial_t(\alpha_{2,0}) + \frac{\alpha_{2,0}\eta_2}{\beta_2}\partial_x(u_{2,0}) = -\nu_{2,1}\left(p_{I,0} - p_{I,0}\right)(\varrho_2 p_{2,2} - \varrho_1 p_{1,0}) \tag{37}$$

From equation (37), we deduce that if $\partial_x u_{2,0} = 0$, $\alpha_{2,0}$ can change only due to boundary conditions. Assuming again periodic or fixed boundary conditions, we retrieve the incompressibility constraint for the weakly compressible phase.

To summarize, in the limit $M_2 \to 0$ we obtain the following limiting equations:

$$\begin{cases} \partial_t \alpha_{1,0} + u_{I,0}\partial_x \alpha_{1,0} & = \nu_{1,2}(\varrho_1 p_{1,0} - \varrho_2 p_{2,2}) \\ \partial_t(\alpha_{1,0}\rho_{1,0}) + \partial_x\left(\alpha_{1,0}\rho_{1,0}u_{1,0}\right) & = 0 \\ \partial_t(\alpha_{1,0}\rho_{1,0}u_{1,0}) + \partial_x\left(\alpha_{1,0}\rho_{1,0}u_{1,0}u_{1,0} + \alpha_{1,0}p_{1,0}\right) & = p_{I,0}\partial_x \alpha_{1,0} + F_{1,2} \\ \partial_t(\alpha_{1,0}\rho_{1,0}E_{1,0}) + \partial_x\left(u_{1,0}(\alpha_{1,0}\rho_{1,0}E_{1,0} + \alpha_{1,0}p_{1,0})\right) & = p_{I,0}u_{I,0}\partial_x \alpha_{1,0} \\ & \quad + u_{I,0}F_{1,2} - \nu_{1,2}p_{I,0}(\varrho_1 p_{1,0} - \varrho_2 p_{2,2}) \\ \partial_t \alpha_{2,0} & = \nu_{2,1}(\varrho_2 p_{2,2} - \varrho_1 p_{1,0}) \\ \partial_t(\alpha_{2,0}\rho_{2,0}) + u_{2,0}\alpha_{2,0}\partial_x\left(\rho_{2,0}\right) & = 0 \\ \partial_t(\alpha_{2,0}\rho_{2,0}u_{2,0}) + \alpha_{2,0}u_{2,0}\partial_x\left(\rho_{2,0}u_{2,0}\right) + \alpha_{2,0}\partial_x(p_{2,2}) & = p_{I,0}\partial_x \alpha_{2,2} + F_{2,1} \\ \partial_x u_{2,0} & = 0, \end{cases} \tag{38}$$

for which the set of well-prepared initial data is:

$$\Psi_{c-i}^{wp} = \left\{ \psi \in \mathbb{R}^{2d+3} : p_{2,0} = p_{2,1} = 0,\ \partial_x u_{2,0} = 0 \right\} \tag{39}$$

It is worth noting that the interface pressure expansion is now:

$$p_I = \alpha_{1,0}p_{1,0} + M_2\alpha_{1,1}p_{1,0} + M_2^2(\alpha_{2,0}p_{2,2} + \alpha_{1,2}p_{1,0}) \tag{40}$$

which suggests that at the interface pressure is governed by the compressible phase (at order $O(1)$ and $O(M_2)$), while secondary effects (order $O(M_2^2)$) are again present due to small imbalances between phasic pressures.

3. All-Mach numerical scheme

In this section, we present the all-Mach numerical scheme which we derive starting from the dimensional form of the equations (1). The derivation of the numerical scheme is articulated in three main steps. First, we introduce a implicit-explicit semi-discretization in time for the stiff and non-stiff part of our equations. Next, we introduce an operator splitting to separate pressure and velocity relaxations from the convective terms, similarly to what is done in [23]. This is presented shortly in sect. 3.2. We show that this leads to a predictor-corrector scheme where first the non-stiff part is solved using an explicit method (predictor), and then a *pressure correction* is added to recover the contribution of acoustic waves (corrector). The pressure correction is found by solving a non-linear elliptic equation for each phasic pressure and is described in sect. 3.2. After introducing the spatial discretization, the resulting numerical scheme is not well-balanced in the sense that steady solutions of continuous equations are not preserved at the discrete level. In order to preserve steady states also in the discrete model, a special discretization for non-conservative terms is introduced in sect. 4.2.1 and 4.2.2.

3.1. IMEX Runge-Kutta time discretization

The first step in the derivation of the all-Mach scheme is the introduction of a suitable time discretization for the convective step, which in compact and dimensional form can be rewritten for any phase k as follows:

$$\partial_t U_k + \partial_x F^{(\text{ns})}(U_k) - G^{(\text{ns})}(U_k) + \epsilon\left(\partial_x F^{(\text{s})}(U_k) - G^{(\text{s})}(U_k)\right) + (1-\epsilon)\left(\partial_x F^{(\text{s})}(U_k) - G^{(\text{s})}(U_k)\right) = R^{(\text{s})}(U_k)$$

where $F^{(\text{s})}$ and $F^{(\text{ns})}$ represent the stiff and non-stiff part of the convective term, $G^{(\text{s})}$ and $G^{(\text{ns})}$ are the stiff and non-stiff part of non-conservative products and $R^{(\text{s})} = R^{(\text{s})}_{(u)} + R^{(\text{s})}_{(p)}$ are the relaxation terms.

$$F^{(\text{ns})} = \begin{bmatrix} 0 \\ \alpha_k\rho_k u_k \\ \alpha_k\rho_k u_k u_k \\ \alpha_k\rho_k u_k K_k \end{bmatrix}, \quad F^{(\text{s})} = \begin{bmatrix} 0 \\ 0 \\ \alpha_k p_k \\ \alpha_k u_k(\rho_k e_k + p_k) \end{bmatrix}, \quad G^{(\text{ns})} = \begin{bmatrix} -u_I\partial_x \alpha_k \\ 0 \\ 0 \\ 0 \end{bmatrix},$$

$$G^{(s)} = \begin{bmatrix} 0 \\ 0 \\ p_I \partial_x \alpha_k \\ p_I u_I \partial_x \alpha_k \end{bmatrix}, \quad R^{(s)}_{(u)} = \begin{bmatrix} 0 \\ 0 \\ \sum_{j\neq k} F_{k,j} \\ u_I \sum_{j\neq k} F_{k,j} \end{bmatrix}$$

$$R^{(s)}_{(p)} = \begin{bmatrix} \sum_{j\neq k} v_{k,j}(p_k - p_j) \\ 0 \\ 0 \\ -\sum_{j\neq k} v_{k,j} p_I (p_k - p_j) \end{bmatrix}.$$

Note that in the above equations, we add and subtract the stiff part of the convective term weighted by a global parameter, $\epsilon := \min(\max_{k,\Omega}(M_k^2(x,t),1))$.

The general idea of our all-Mach derivation is to treat terms multiplied by $(1-\epsilon)$ and relaxation terms in an implicit fashion, while terms multiplied by ϵ and non-stiff terms are kept explicit. Using this device, when the most compressible phase approaches the incompressible limit (i.e. $\epsilon \to 0$) the contribution of stiff terms to the explicit part of the scheme vanishes and we are left with a fully implicit treatment of acoustic waves. On the contrary, when $M_k^2 \geq 1$, the contribution from stiff terms to the implicit part of the scheme disappears, and we revert to fully explicit scheme for compressible flows.

In theory, one could resort to a more standard implicit-explicit discretization where only the stiff terms are treated implicitly while non-stiff terms are kept fully explicit. In practice, we observed that such a numerical scheme possesses poor stability properties. When one (or both phases) enter a transitional regime, spurious oscillations appear in the numerical solution. The reason of this behavior is yet to be fully understood.

To obtain a semidiscrete scheme for the convective step, we integrate in time the above system of equations using an IMEX-RK method ([22]). For a general IMEX-RK scheme with s stages we obtain:

$$\begin{aligned} U_k^{n+1} &= U_k^n \\ &- \Delta t \sum_{l=1}^{s} \tilde{b}_l \left[\partial_x F^{(\mathrm{ns})}(U_k^{(l)}) - G^{(\mathrm{ns})}(U_k^{(l)}) + \epsilon \left(\partial_x F^{(\mathrm{s})}(U_k^{(l)}) - G^{(\mathrm{s})}(U_k^{(l)}) \right) \right] \\ &- \Delta t \sum_{l=1}^{s} b_l \left[(1-\epsilon) \left(\partial_x F^{(\mathrm{s})}(U_k^{(l)}) - G^{(\mathrm{s})}(U_k^{(l)}) \right) - R^{(\mathrm{s})}(U_k^{(l)}) \right] \end{aligned} \tag{41}$$

where the solution at intermediate stages, $U_k^{(l)}$ $(l = 1, \dots, s)$ is given by:

$$\begin{aligned} U_k^{(l)} &= U_k^n \\ &- \Delta t \sum_{m=1}^{l-1} \tilde{a}_{l,m} \left[\partial_x F^{(\mathrm{ns})}(U_k^{(m)}) - G^{(\mathrm{ns})}(U_k^{(m)}) \right. \\ &\qquad \left. + \epsilon \left(\partial_x F^{(\mathrm{s})}(U_k^{(m)}) - G^{(\mathrm{s})}(U_k^{(m)}) \right) \right] \\ &- \Delta t \sum_{m=1}^{l} a_{l,m} \left[(1-\epsilon) \left(\partial_x F^{(\mathrm{s})}(U_k^{(m)}) - G^{(\mathrm{s})}(U_k^{(m)}) \right) - R^{(\mathrm{s})}(U_k^{(m)}) \right] \end{aligned} \tag{42}$$

Here, $\left(\tilde{a}_{l,m}, \tilde{b}_l\right)$ and $\left(a_{l,m}, b_l\right)$ are the coefficients for the explicit and implicit part of the Butcher's tableaux:

$$\begin{array}{c|c} \tilde{c} & \tilde{a} \\ \hline & \tilde{b} \end{array} \qquad \begin{array}{c|c} c & a \\ \hline & b \end{array} \tag{43}$$

With the above choices, the CFL condition becomes:

$$\Delta t \leq C \frac{\Delta x}{\max_{k,\Omega}(|u_k| + \epsilon c_k)}, \tag{44}$$

which depends only on the macroscopic velocity when all the phases approach the incompressible limit.

3.2. Splitting and elliptic equation for the implicit step

Eqs. (42) require to solve a system of non-linear equations in the unknown conservative variables at each time step for each intermediate stage of the RK method. Obviously, this has almost the same computational complexity of a fully implicit method. In this section, we show that under some mild assumptions, a predictor-corrector scheme can be derived from (41) and (42).

Given $U^{(m)}, m = 1, \dots, l-1$, our task is to compute the intermediate solution $U^{(l)}$ at stage l. Since the stiff part of the convective term for the mass equation is identically zero, $(\alpha\rho)_k^{(l)}$ can be readily obtained as follows:

$$(\alpha\rho)_k^{(l)} = (\alpha\rho)_k^n - \Delta t \sum_{m=1}^{l-1} \tilde{a}_{l,m} \partial_x F^{(ns,\alpha\rho)}(U_k^{(m)}) \tag{45}$$

where $F^{(ns,\alpha\rho)}$ is used to indicate the component of the non-stiff part of the convective term corresponding to the mass equation.

Next, equations for momentum and energy can be rewritten as:

$$\begin{aligned} (\alpha\rho u)_k^{(l)} &= (\alpha\rho u)_k^* - \Delta t\, a_{l,l}(1-\epsilon) \left(\partial_x F^{(s,\alpha\rho u)}(U_k^{(l)}) - G^{(s,\alpha\rho u)}(U_k^{(l)}) \right) \\ &\quad + \Delta t\, a_{l,l} R^{(s,\alpha\rho u)}(U_k^{(l)}) \end{aligned} \tag{46a}$$

$$\begin{aligned} (\alpha\rho E)_k^{(l)} &= (\alpha\rho E)_k^* - \Delta t\, a_{l,l}(1-\epsilon) \left(\partial_x F^{(s,\alpha\rho E)}(U_k^{(l)}) - G^{(s,\alpha\rho E)}(U_k^{(l)}) \right) \\ &\quad + \Delta t\, a_{l,l} R^{(s,\alpha\rho E)}(U_k^{(l)}) \end{aligned} \tag{46b}$$

where:

$$\begin{aligned} (\alpha\rho u)_k^* &:= (\alpha\rho u)_k^n - \Delta t\, S^{(l-1,\alpha\rho u)} \\ (\alpha\rho E)_k^* &:= (\alpha\rho E)_k^n - \Delta t\, S^{(l-1,\alpha\rho E)} \end{aligned} \tag{47}$$

and $S^{(l-1,\cdot)}$ is a shorthand notation for:

$$\begin{aligned} S^{(l-1,\cdot)} &:= \sum_{m=1}^{l-1} \tilde{a}_{l,m} \left[\partial_x F^{(ns,\cdot)}(U_k^{(m)}) - G^{(ns,\cdot)}(U_k^{(m)}) \right. \\ &\qquad \left. + \epsilon \left(\partial_x F^{(s,\cdot)}(U_k^{(m)}) - G^{(s,\cdot)}(U_k^{(m)}) \right) \right] \\ &\quad + \sum_{m=1}^{l-1} a_{l,m} \left[(1-\epsilon) \left(\partial_x F^{(s,\cdot)}(U_k^{(m)}) - G^{(s,\cdot)}(U_k^{(m)}) \right) \right. \\ &\qquad \left. - R^{(s,\cdot)}(U_k^{(m)}) \right] \end{aligned} \tag{48}$$

We can now rewrite the full system for the implicit step as follows:

$$\frac{U_k^{(l)} - U_k^*}{\Delta t} = -a_{l,l}(1-\epsilon) \left(\partial_x F^{(s)}(U_k^{(l)}) - G^{(s)}(U_k^{(l)}) \right) + a_{l,l} R^{(s)}(U_k^{(l)}) \tag{49}$$

Note that at stage l, $S^{(l-1,\cdot)}$ only depends on the (known) solution at previous Runge-Kutta stages, $m = 1, \dots, l-1$. Additionally, note that state $U_k^* = (\alpha_k^*, (\alpha\rho)_k^{(l)}, (\alpha\rho u)_k^*, (\alpha\rho E)_k^*)$ is completely determined except for α^*. For now, we assume that α^* is known. In later sections, we will show that the choice of state α^* cannot be arbitrary if one wishes to recover a well-balanced scheme.

At this point, we apply a succession of operators (Strang splitting [28]) to the semi-discrete system (49). Given the solution vector U_k^*, we compute $U_k^{(l)}$ as follows:

$$U_k^{(l)} = \mathcal{C}^{\Delta t} \mathcal{R}^{\Delta t} U_k^* \tag{50}$$

i.e. we firstly apply the relaxation operator $\mathcal{R}_{\Delta t}$, and then we use the solution of the relaxation step as the initial condition to solve the convective operator. In (50), we introduced a first order operator splitting. Second order accuracy in time can be achieved using Strang's splitting ([28]):

$$U_k^{(l)} = \mathcal{R}^{\Delta t/2}\mathcal{C}^{\Delta t}\mathcal{R}^{\Delta t/2}U_k^*.$$

The relaxation step, in turn, is split into velocity and pressure relaxation steps, i.e.:

$$\mathcal{R}^{\Delta t} := \mathcal{R}_{(u)}^{\Delta t}\,\mathcal{R}_{(p)}^{\Delta t}$$

Denoting $U_k^{(nr)}$ a general non-relaxed state before any operator and $U_k^{(r)}$ the relaxed state after the operator, the velocity and pressure relaxations are given by:

$$\mathcal{R}_{(u)}: \frac{U_k^{(r)} - U_k^{(nr)}}{\Delta t} = a_{l,l}R_{(u)}^{(s)}(U_k^{(r)}) \tag{51}$$

and:

$$\mathcal{R}_{(p)}: \frac{U_k^{(r)} - U_k^{(nr)}}{\Delta t} = a_{l,l}R_{(p)}^{(s)}(U_k^{(r)}) \tag{52}$$

Note that both (51) and (52) represent a system of discrete (non)linear ODEs that are integrated locally in each computational cell with an implicit scheme.

At this point, we can proceed with the solution of the convective operator $\mathcal{C}^{\Delta t}$. We denote with U_k^{**} the vector of conserved variables after relaxation operators and write $\mathcal{C}^{\Delta t}$ as follows:

$$U_k^{(l)} = U_k^{**} - \Delta t a_{l,l}(1-\epsilon)\left(\partial_x F^{(s)}(U_k^{(l)}) - G^{(s)}(U_k^{(l)})\right) \tag{53}$$

As pointed out in the introduction, we are mostly interested in two-phase flows characterized by slow transient dynamics and weak thermodynamic disequilibrium. Therefore, in the energy equation the contribution of kinetic energy on the l.h.s., total enthalpy flux and the work done by interface pressure forces can be linearized around state $U_k^{**} = (\alpha_k^{**}, (\alpha\rho)_k^{(l)}, (\alpha\rho u)_k^{**}, (\alpha\rho E)_k^{**})$.

Eq. (46b) can now be written as:

$$(\alpha\rho e)_k^{(l)} + (\alpha\rho K)_k^{(l)} = (\alpha\rho E)_k^{**} - \Delta t\, a_{l,l}(1-\epsilon)\left[\partial_x(H_k^{(l)}(\alpha\rho u)_k^{(l)}) - u_I^{(l)}p_I^{(l)}\partial_x\alpha_k^{(l)}\right] \tag{54}$$

and applying the linearization, we obtain:

$$(\alpha\rho e)_k^{(l)} + \frac{1}{2}\frac{(\alpha\rho u)_k^{**}}{(\alpha\rho)_k^{**}}(\alpha\rho u)_k^{(l)} = (\alpha\rho E)_k^{**} - \Delta t\, a_{l,l}(1-\epsilon)\left[\partial_x(H_k^{**}(\alpha\rho u)_k^{(l)}) - u_I^{**}p_I^{(l)}\partial_x\alpha_k^{**}\right]. \tag{55}$$

Next, we write momentum equation for the convection operator as:

$$(\alpha\rho u)_k^{(l)} = (\alpha\rho u)_k^{**} - \Delta t\, a_{l,l}(1-\epsilon)\left[\partial_x(\alpha_k^{(l)}p_k^{(l)}) - p_I^{(l)}\partial_x\alpha_k^{(l)}\right] \tag{56}$$

and substituting it in equation (55) and rearranging terms, we get:

$$(\alpha\rho e)_k^{(l)} + \frac{1}{2}\chi u_k^{**}\left(-\partial_x(\alpha p)_k^{(l)} + p_I^{(l)}\partial_x\alpha_k^{(l)}\right) - \chi u_I^{**}p_I^{(l)}\partial_x\alpha_k^{**} + \chi^2\partial_x\left[H_k^{**}\left(-\partial_x(\alpha p)_k^{(l)} + p_I^{(l)}\partial_x\alpha_k^{(l)}\right)\right] = (\alpha\rho e)_k^{**} - \chi\,\partial_x\left((\alpha\rho u)_k^{**}H_k^{**}\right) \tag{57}$$

where $\chi = a_{l,l}\Delta t(1-\epsilon)$.

Assuming a general form for the EOS of each phase, (57) represents a system of non-linear elliptic equations in the unknown phasic pressures, p_k, $k = 1, 2$ which are coupled through the interface pressure, p_I. The above system of equations can be solved efficiently using, for instance, Picard's method. In case of perfect gasses (or stiffened EOS) the above system of equations become linear, and can be solved by resorting to any numerical method for linear elliptic equations.

Note that the procedure outlined in this section represents *de-facto* a predictor-corrector scheme. First conservative variables are computed by neglecting the implicit part of the convective term as shown by eqs. (45) and (47) (predictor). Next relaxation operators are applied to the system. Then, new values for phasic pressures are obtained by solving a system of coupled non-linear elliptic equations (corrector). Finally, the *pressure correction* is applied as shown by eqs. (56) and (55).

Lastly, note that the above linearizations do not play any role in the highly compressible regime, as the implicit part vanishes for $\epsilon \to 1$. In practice, we were able to simulate flows characterized by moderate to fast transient dynamics. In a few cases, we observed spurious oscillations in the numerical solution which were dealt with using a device similar to the one employed in fully implicit schemes. We started the computation with $\epsilon = 1$ (fully explicit scheme), resulting in a CFL condition based on the speed of acoustic perturbations, and then we increased ϵ to $\min(\max_k(\max_\Omega M_k^2(x,t)), 1)$ over few dozens of iterations.

The above procedure can be further simplified when relaxation rates are either instantaneous or equal to zero (no relaxation applied). This is a relevant and common assumption for practical problems. In particular, when interfaces are present in the problem, if relaxation rates are not assumed to be instantaneous, the model would fail at the second time step since boundary conditions would not be guaranteed at the interface (see [23] for a more detailed discussion).

In the case relaxations of pressures or velocities are absent, we have $\tau_{k,j} = 0$ and/or $\nu_{k,j} = 0$. It follows that in all the equations the corresponding source terms disappear. On the other hand, in the case of instantaneous relaxation rates, we have $\tau_{k,j} \to \infty$ and/or $\nu_{k,j} \to \infty$ and the solution procedure can be simplified as detailed in the following paragraphs.

It is worth mentioning that when instantaneous pressure relaxation is applied, we obtain the 6-equation model with single pressure and two-velocities mentioned in the introduction. In some circumstances, the 6-equation model presents complex eigenvalues and is ill-posed. In those cases, instabilities can arise in the solution. However, it is possible to solve our system with very large values of $\nu_{k,j}$, which formally leads to a well-posed system and approximates the instantaneous relaxation procedure. At the numerical level this does not pose a particular challenge, since an implicit scheme is used to advance in time both velocity and pressure relaxation operators.

Instantaneous pressure relaxation

When $\nu_{k,j} \to \infty$ (instantaneous pressure relaxation), thermodynamic relaxation is characterized by a time scale much smaller than the advection time scale. In such cases, eqs. (52) reduce to a system of non-linear algebraic equations which are solved to obtain the common pressure value, p^r, and a new value for volumetric fractions (details can be found in [23]):

$$\begin{cases} e_k^r = e_k^{nr} - \frac{1}{2}\frac{(p^r + p_I^n)}{(\alpha\rho)_k^{nr}}(\alpha_k^r - \alpha_k^{nr}) \\ p^r = p_k(e_k^r, \rho_k^r) \\ \alpha_k^r\rho_k^r = (\alpha\rho)_k^{nr} \\ \sum_k \alpha_k^r = 1 \end{cases}, \quad \forall\, k = 1, \dots, n_p \tag{58}$$

Moreover, we can solve equation (57) for a common pressure value. This is done performing summation over k obtaining:

$$\sum_k (\alpha\rho e)_k^{(l)} - \frac{\chi}{2}\sum_k (u_k^{**}\alpha_k^{(l)}\partial_x p^{(l)}) - \chi^2\sum_k\left[\partial_x\left(H_k^{**}\alpha_k^{(l)}\partial_x p^{(l)}\right)\right] = \sum_k\left[(\alpha\rho e)_k^{**} - \chi\,\partial_x(\alpha\rho u)_k^{**}H_k^*\right] \tag{59}$$

which requires to solve only a single (non-linear) elliptic equation at each stage of the RK method to compute the common pressure, $p^{(l)}$, at the l-th stage of the Runge-Kutta method. As for (57), in case of perfect gasses (or stiffened EOS), the above system of equations become linear. Finally, momentum can be updated using equation (56), from which we retrieve the values of the velocities and update also the total energy using its definition.

Instantaneous velocity relaxation

The case when $\tau_{k,j} \to \infty$ (instantaneous velocity relaxation), corresponds to large friction forces acting at the interface between phases

k and j. In such situations, the solution of velocity relaxation operator (51) becomes trivial and both velocities u_k^{nr} and u_j^{nr} are instantaneously homogenized to the common value u^r (see [23]):

$$u_k^r = u_j^r = u^r = \frac{(\alpha\rho u)_k^{nr} + (\alpha\rho u)_j^{nr}}{(\alpha\rho)_k^{nr} + (\alpha\rho)_j^{nr}}. \tag{60}$$

In this case, elliptic pressure equation (57) is employed to evaluate the pressure fields at state l. At this point, using the fact that $(\alpha_k\rho_k)^{(l)} = (\alpha_k\rho_k)^{**}$, we rewrite the equation for the momentum update (56) as:

$$(\alpha_k\rho_k)^{**}u^{(l)} = (\alpha_k\rho_k u_k)^{**} - \chi\left(\partial_x(\alpha_k p_k)^{(l)} - p_I^{(l)}\partial_x\alpha_k^{(l)}\right). \tag{61}$$

We now add momentum equations for phase 1 and 2 to solve for a common velocity. Rearranging, we obtain:

$$u^{(l)} = \frac{(\alpha_1\rho_1u_1)^{**} + (\alpha_2\rho_2u_2)^{**} - \chi\partial_x(\alpha_1^{(l)}p_1^{(l)} + \alpha_2^{(l)}p_2^{(l)})}{(\alpha_1\rho_1)^{**} + (\alpha_2\rho_2)^{**}}. \tag{62}$$

Finally, knowing all the primitive variables at state l, we can update energy using its definition.

4. Fully discrete model

The last ingredient required for the numerical resolution of eqs. (41) and (42) is the space discretization. To keep notation compact, we focus on the one-dimensional case, where the domain of interest Ω is discretized in N cells of width Δx, indexed by j.

4.1. Spatial discretization

Discretization of the explicit part of (41) follows the standard finite volume formalism, where we denote by $U_{k,j}^n$ the vector of cell averages of conservative variables for phase k at cell j at time step t^n. The fully discrete version of eq. (41) reads as follows:

$$\begin{aligned}
U_{k,j}^{n+1} &= U_{k,j}^n \\
&-\Delta t\sum_{l=1}^{s}\tilde{b}_l\left[\frac{(\mathcal{F}_{k,j+1/2}^{(ns),(l)} - \mathcal{F}_{k,j-1/2}^{(ns),(l)})}{\Delta x} - G_{k,j}^{(ns),(l)}\right. \\
&\qquad\left.+\epsilon\frac{(\mathcal{F}_{k,j+1/2}^{(s),(l)} - \mathcal{F}_{k,j-1/2}^{(s),(l)})}{\Delta x} - \epsilon G_{k,j}^{(s),(l)}\right] \\
&-\Delta t\sum_{l=1}^{s}b_l\left[(1-\epsilon)\frac{(F_{k,j+1}^{(s),(l)} - F_{k,j-1}^{(s),(l)})}{2\Delta x} - (1-\epsilon)G_{k,j}^{(s),(l)} - R_{k,j}^{(s),(l)}\right]
\end{aligned} \tag{63}$$

where $\mathcal{F}_{k,j+1/2}^{l}$ is the numerical flux function evaluated at cell interface $j \pm 1/2$ using the solution at stage l of the IMEX-RK method, while $G_{k,j}^{(s)} = H_{k,j}^{(s)}\Delta_{k,j}^{wb}$, $H_{k,j}^{(s)} = (0, 0, p_I, p_I u_I)^T$ and $G_{k,j}^{(ns)} = ((-u_I\partial_x\alpha_k)_j, 0, 0, 0)^T$ are the discrete counterpart of the stiff and non-stiff part of non-conservative terms.

Here, we introduce Δ^{wb} to indicate a suitable discretization of $\partial_x\alpha_k$. Both Δ^{wb} and the discretization of the volumetric fraction equation must be chosen in such a way that the resulting numerical scheme is well-balanced. As shown in the next section, a well-balanced discretization of non-conservative terms strongly depends on the numerical flux function chosen for the convective term. Although the derivation presented in the next sections can be applied to more general flux functions, for the sake of brevity, we focus only on Rusanov's and HLL (Harten, Lax and van Leer [29]) numerical fluxes.

Rusanov's fluxes are given by:

$$\mathcal{F}_{k,j+1/2}^{\text{Rusanov}} = \frac{1}{2}[F(U_{k,j+1/2^+}) + F(U_{k,j+1/2-}) - s_{j+1/2}(U_{j+1/2^+} - U_{j+1/2^-})] \tag{64}$$

where $U_{j+1/2^\pm}$ denotes the value of the solution reconstructed at the right/left of cell interface $j+1/2$, and $s_{j+1/2}$ is an estimate of the wave speed. In this work, we adopt $s_{j+1/2} = \max(s_{j+1/2^-}, s_{j+1/2^+})$, where $s_{j+1/2^-} = \max_k \max(|\lambda_{k,j+1/2^-}^-|, |\lambda_{k,j+1/2^-}^+|)$ and $s_{j+1/2^+} = \max_k \max(|\lambda_{k,j+1/2^+}^-|, |\lambda_{k,j+1/2^+}^+|)$ (see [30]).

HLL numerical fluxes are given by:

$$\begin{aligned}
\mathcal{F}_{k,j+1/2}^{HLL} = &\frac{s_{j+1/2}^+F(U_{k,j+1/2^-}) - s_{j+1/2}^-F(U_{k,j+1/2^+})}{s^+ - s^-} \\
&+\frac{s_{j+1/2}^+s_{j+1/2}^-(U_{k,j+1/2^+} - U_{,j+1/2^-})}{s^+ - s^-}
\end{aligned} \tag{65}$$

where the following estimates for $s_{j+1/2}^+$ and $s_{j+1/2}^-$ are used (see [29] or [31]):

$$s_{j+1/2}^+ = \max_k\ \max\left\{0, \lambda_{k,j+1/2^+}^+, \lambda_{k,j+1/2^-}^+\right\},$$
$$s_{j+1/2}^- = \min_k\ \min\left\{0, \lambda_{k,j+1/2^+}^-, \lambda_{k,j+1/2^-}^-\right\}$$

As usual, values of conservative variables at right/left of the cell interface are reconstructed from cell averages. For a first order scheme, a piece-wise constant reconstruction is employed, that is:

$$U_j(x, t^n) = U_j^n \qquad \text{for } x_{j-1/2} < x < x_{j+1/2}. \tag{66}$$

Second order accuracy in space can be achieved by using a piece-wise linear reconstruction, i.e.:

$$q_j(x, t^n) = q_j^n + \sigma_j^n(x - x_j) \qquad \text{for } x_{j-1/2} < x < x_{j+1/2}, \tag{67}$$

where q is the reconstructed variable, and the slope of the reconstruction is estimated from cell average quantities as follows:

$$\sigma_j^n = \frac{(q_{j+1}^n - q_j^n)}{\Delta x}\phi(\theta_j^n) \quad \text{with} \quad \theta_j^n = \frac{q_j^n - q_{j-1}^n}{q_{j+1}^n - q_j^n} \tag{68}$$

As customary, we introduced a slope limiter function, ϕ, to ensure that the resulting scheme is total variation diminishing (TVD). In our numerical experiment, we reconstructed primitive variables and we considered the minmod limiter function:

$$\phi_{\text{minmod}}(\theta) = \begin{cases} \min(\theta, 1) & \text{if } \theta > 0 \\ 0 & \text{if } \theta \le 0 \end{cases} \tag{69}$$

or the van Leer's slope limiter:

$$\phi_{\text{van Leer}}(\theta) = \frac{\theta + |\theta|}{1 + |\theta|}. \tag{70}$$

Lastly, in the elliptic pressure equation (57) (or (59)), we use central finite differences to approximate first and second order derivatives as follows:

$$\begin{aligned}
\partial_x q|_j &\approx (\Delta q)_j = \frac{q_{j+1} - q_{j-1}}{2\Delta x} \\
\partial_x(z\partial_x q)|_j &\approx (\Delta(z\Delta q))_j = \frac{1}{2\Delta x^2}\Big[q_{j+1}(z_j + z_{j+1}) - q_j(z_{j-1} + 2z_j + z_{j+1}) \\
&\qquad + q_{j-1}(z_{j-1} + z_j)\Big].
\end{aligned} \tag{71}$$

4.2. Well-balancing

A naive discretization of non-conservative terms leads to a numerical scheme which is incapable of preserving steady states. The problem of balancing equations has been studied in literature for various model equations (see for instance, [32], [33], [34], [35], [36] and [37]). However, in the case of Baer-Nunziato model, a well balanced discretization of non-conservative terms is particularly tricky as it appears that it is not possible to recover a well-balanced scheme capable of preserving all classes of steady state solutions.

In this work, we focus only on one class of steady solutions, which is defined by the following relationships:

$$\begin{aligned} &\frac{\partial \alpha_k}{\partial t} + u\frac{\partial \alpha_k}{\partial x} = 0, \\ &\frac{\partial \rho_k}{\partial t} + u\frac{\partial \rho_k}{\partial x} = 0, \qquad \frac{\partial u_k}{\partial t} = 0, \qquad \frac{\partial p_k}{\partial t} = 0, \end{aligned} \tag{72}$$

which is derived from the original model of equations (1) in the case $u_1 = u_2 = u_I = u$ and $p_1 = p_2 = p_I = p$. The above conditions imply that a contact discontinuity between two phases moving with a constant flow velocity is preserved. Note that the case of fixed contact discontinuity (the so-called *lake-at-rest* condition) is a special case corresponding to $u \equiv 0$. In order to recover a well-balanced scheme, the explicit part of our numerical scheme (i.e. stiff and non-stiff terms multiplied by ϵ) and the implicit part (stiff terms multiplied by $(1-\epsilon)$) are balanced independently. For the sake of clarity, in what follows we assume that primitive variables are reconstructed at first order and that all phases are governed by the stiffened gas EOS. Moreover, pressure and velocity relaxation terms are not involved in the balancing procedure since they are identically zero. This is due to the fact that for the class steady-states of interest $u_1 = u_2 = u$ and $p_1 = p_2 = p$. Consequently $\nu(p_1 - p_2) = 0$ and $\tau(u_1 - u_2) = 0$ and also $U^{**} = U^*$. The same derivation can be followed also for second order reconstruction.

In what follows, we omit the phase index k for clarity. The same procedure can be carried out for each phase independently.

4.2.1. Explicit step balancing

The derivation of a well-balanced discretization for non conservative terms in the explicit part of the numerical scheme follows the same steps as in [23], so we omit the details here. In short, to balance the explicit terms in eq. (42) for any intermediate stage $U^{(l)}$ $(l = 1, \dots, s)$, we write the discrete explicit part of eq. (42) as follows:

$$\begin{aligned} U_j^{(l)} = U_j^n - \Delta t \sum_{m=1}^{l-1} \tilde{a}_{l,m} \Bigg[&\frac{(\mathcal{F}_{j+1/2}^{(ns),(m)} - \mathcal{F}_{j-1/2}^{(ns),(m)})}{\Delta x} - G_j^{(ns),(m)} \\ &+\epsilon \frac{(\mathcal{F}_{j+1/2}^{(s),(m)} - \mathcal{F}_{j-1/2}^{(s),(m)})}{\Delta x} - \epsilon G_j^{(s),(m)} \Bigg] \end{aligned} \tag{73}$$

and we define:

$$U_j^{(i)} = U_j^n - \Delta t\, S_j^{(i-1)} \tag{74}$$

where $S_j^{(i-1)}$ depends only on the solution computed at the previous stages of a Runge-Kutta method, that is:

$$\begin{aligned} S_j^{(i-1)} := \sum_{m=1}^{i-1} \tilde{a}_{l,m} \Bigg[&\frac{(\mathcal{F}_{j+1/2}^{(ns),(m)} - \mathcal{F}_{j-1/2}^{(ns),(m)})}{\Delta x} - G_j^{(ns),(m)} \\ &+\epsilon \frac{(\mathcal{F}_{j+1/2}^{(s),(m)} - \mathcal{F}_{j-1/2}^{(s),(m)})}{\Delta x} - \epsilon G_j^{(s),(m)} \Bigg]. \end{aligned} \tag{75}$$

Using this notation, $U_j^{(i)}$ can be written as follows:

$$\begin{aligned} U_j^{(i)} = U_j^{(i-1)} - \Delta t\, \tilde{a}_{l,i-1} \Bigg[&\frac{(\mathcal{F}_{j+1/2}^{(ns),(i-1)} - \mathcal{F}_{j-1/2}^{(ns),(i-1)})}{\Delta x} - G_j^{(ns),(i-1)} \\ &+\epsilon \frac{(\mathcal{F}_{j+1/2}^{(s),(i-1)} - \mathcal{F}_{j-1/2}^{(s),(i-1)})}{\Delta x} - \epsilon G_j^{(s),(i-1)} \Bigg] \end{aligned} \tag{76}$$

Next, we substitute the discrete mass equation into the discrete momentum equation and we use the fact that in the class of steady state solutions (72) we have:

$$\begin{aligned} &u_{k,j}^{(i)} = u_{I,j}^{(i)} = u \qquad \forall k, j, i \\ &p_{k,j}^{(i)} = p_{I,j}^{(i)} = p \qquad \forall k, j, i \end{aligned} \tag{77}$$

Using the above conditions, one obtains a different expression for Δ^{wb} depending on the particular choice of the numerical flux function.

For Rusanov fluxes, we obtain:

$$\Delta_j^{wb} = \frac{\left(\alpha_{j+1}^{(i-1)} - \alpha_{j-1}^{(i-1)}\right)}{2\Delta x}. \tag{78}$$

While for HLL fluxes, Δ^{wb} reads as follows:

$$\Delta_j^{wb} = \frac{1}{\Delta x} \left\{ \frac{s_{j+1/2}^+ \alpha_j^{(i-1)} - s_{j+1/2}^- \alpha_{j+1}^{(i-1)}}{s_{j+1/2}^+ - s_{j+1/2}^-} - \frac{s_{j-1/2}^+ \alpha_{j-1}^{(i-1)} - s_{j-1/2}^- \alpha_j^{(i-1)}}{s_{j-1/2}^+ - s_{j-1/2}^-} \right\} \tag{79}$$

Discretization of non conservative terms given by (78) (and (79)) is not sufficient alone to obtain a well-balanced scheme. When substituting (78) (or (79)) and the discrete momentum equation inside the discrete energy equation, one finds that in order to preserve a steady pressure (i.e. $p_j^{(i)} = p_j^{(i-1)} = p$), volumetric fractions must be updated as follows (Rusanov fluxes):

$$\begin{aligned} \alpha_j^{(i)} = \alpha_j^{(i-1)} - \tilde{a}_{l,i-1} \frac{\Delta t}{2\Delta x} \Big[&\epsilon u_j^{(i-1)} \left(\alpha_{j+1}^{(i-1)} - \alpha_{j-1}^{(i-1)}\right) \\ &- s_{j+1/2} \left(\alpha_{j+1}^{(i-1)} - \alpha_j^{(i-1)}\right) \\ &+ s_{j-1/2} \left(\alpha_j^{(i-1)} - \alpha_{j-1}^{(i-1)}\right) \Big], \end{aligned} \tag{80}$$

or using (HLL fluxes):

$$\begin{aligned} \alpha_j^{(i)} = \alpha_j^{(i-1)} - \tilde{a}_{l,i-1} \frac{\Delta t}{\Delta x} \\ \Bigg\{ u_j^{(i-1)} \frac{\left[\epsilon \left(s_{j+1/2}^+ \alpha_j^{(i-1)} - s_{j+1/2}^- \alpha_{j+1}^{(i-1)}\right) + s_{j+1/2}^+ s_{j+1/2}^- \left(\alpha_{j+1}^{(i-1)} - \alpha_j^{(i-1)}\right)\right]}{s_{j+1/2}^+ - s_{j+1/2}^-} \\ - u_j^{(i-1)} \frac{\left[\epsilon \left(s_{j-1/2}^+ \alpha_{j-1}^{(i-1)} - s_{j-1/2}^- \alpha_j^{(i-1)}\right) + s_{j-1/2}^+ s_{j-1/2}^- \left(\alpha_j^{(i-1)} - \alpha_{j-1}^{(i-1)}\right)\right]}{s_{j-1/2}^+ - s_{j-1/2}^-} \Bigg\}. \end{aligned} \tag{81}$$

Note that in (80) (and (81)), an additional numerical diffusion term appears, which seems to be unavoidable in order to obtain a well-balanced scheme.

Discretization of non conservative terms given by eqs. (78) (or (79)) and (80) (or (81)) ensures that for each intermediate stage of the Runge-Kutta method the explicit part is well-balanced. From here, it is straightforward to show that the overall explicit part of the numerical scheme is also well-balanced. In the next subsection, we verify that, with the discrete operators introduced so far, the steady states of interest are preserved also for the elliptic pressure equation and the implicit part of the scheme.

4.2.2. Elliptic equation and implicit step balancing

In order to recover a well-balanced scheme, also the implicit part of the numerical scheme must be balanced. We now verify that, using the discretization introduced in subsection 4.1, the class of steady states of interest are preserved also for the elliptic equation and for the implicit step. The discrete pressure equation for a generic phase k at the steady state reads as follows (phase subscript omitted):

$$\begin{aligned}
&\underbrace{(\alpha\rho e)_j^{(l)}}_{I} + \underbrace{\chi\frac{u_j^{**}}{2}\left(-p_j^{(l)}(\Delta\alpha^{(l)})_j + p_{I,j}^{(l)}(\Delta\alpha^{(l)})_j\right)}_{II} \\
&\quad + \underbrace{\chi^2\left[-(\Delta(H^{**}p^{(l)}\Delta\alpha^{(l)}))_j + (\Delta(H^{**}p_I^{(l)}\Delta\alpha^{(l)}))_j\right]}_{III} \\
&\quad \underbrace{-\chi u_{I,j}^{**}p_{I,j}^{(l)}(\Delta\alpha^{**})_j}_{IV} = \underbrace{(\alpha\rho e)_j^{**}}_{V} \underbrace{-\chi\left(\Delta(\alpha\rho u)^{**}e^{**}\right)_j}_{VI} \\
&\quad \underbrace{-\chi\left(\Delta(\alpha\rho u)^{**}\frac{p^{**}}{\rho^{**}}\right)_j}_{VII}.
\end{aligned} \tag{82}$$

Using the fact that at steady state $p_j^{(l)} = p_{I,j}^{(l)} = p_j^{**} = p$ and $u_j^{(l)} = u_{I,j}^{(l)} = u_j^{**} = u$, terms II and III are equal to zero and also IV cancels out with VII. So we are left with:

$$(\alpha\rho e)_j^{(l)} = (\alpha\rho e)_j^{**} - a_{l,l}\Delta t(1-\epsilon)u_j^{**}\frac{((\alpha\rho e)_{j+1}^{**} - (\alpha\rho e)_{j-1}^{**})}{2\Delta x}. \tag{83}$$

Substituting the equation of state for stiffened gasses, we have:

$$(\frac{p^{(l)}}{\beta} + \frac{\eta}{\beta})\alpha_j^{(l)} = (\frac{p^{**}}{\beta} + \frac{\eta}{\beta})\alpha_j^{**} - (\frac{p^{**}}{\beta} + \frac{\eta}{\beta})a_{l,l}\Delta t(1-\epsilon)u_j^{**}\frac{(\alpha_{j+1}^{**} - \alpha_{j-1}^{**})}{2\Delta x}, \tag{84}$$

which shows that in order to preserve the steady state solution, volumetric fractions must be updated as follows:

$$\alpha_j^{(l)} = \alpha_j^{**} - a_{l,l}\Delta t(1-\epsilon)u_j^{**}\frac{(\alpha_{j+1}^{**} - \alpha_{j-1}^{**})}{2\Delta x}. \tag{85}$$

Summing up eqs. (80) (or (81)) and (85), we obtain the numerical scheme which must be used to update volumetric fractions. If the Rusanov scheme is used to compute conservative fluxes, we obtain:

$$\begin{cases}
\alpha_j^* = \alpha_j^n - \Delta t\sum_{m=1}^{l-1}\tilde{a}_{l,m}\Big\{-\frac{1}{2\Delta x}\big[\epsilon u_j^{(m)}\left(\alpha_{j+1}^{(m)} - \alpha_{j-1}^{(m)}\right) \\
\qquad\qquad - s_{j+1/2}\left(\alpha_{j+1}^{(m)} - \alpha_j^{(m)}\right) + s_{j-1/2}\left(\alpha_j^{(m)} - \alpha_{j-1}^{(m)}\right)\big]\Big\}, \\
\alpha_j^{(l)} = \alpha_j^{**} - a_{l,l}\frac{\Delta t}{2\Delta x}(1-\epsilon)u_j^{**}(\alpha_{j+1}^{**} - \alpha_{j-1}^{**}).
\end{cases} \tag{86}$$

For the case of HLL fluxes, the rule to update volumetric fraction becomes:

$$\begin{cases}
\alpha_j^* = \alpha_j^n - \Delta t\sum_{m=1}^{l-1}\tilde{a}_{l,m} \\
\Big\{-\frac{1}{\Delta x}\Big[u_j^{(m)}\frac{[\epsilon(s_{j+1/2}^+\alpha_j^{(m)} - s_{j+1/2}^-\alpha_{j+1}^{(m)}) + s_{j+1/2}^+s_{j+1/2}^-(\alpha_{j+1}^{(m)} - \alpha_j^{(m)})]}{s_{j+1/2}^+ - s_{j+1/2}^-} \\
- u_j^{(m)}\frac{[\epsilon(s_{j-1/2}^+\alpha_{j-1}^{(m)} - s_{j-1/2}^-\alpha_j^{(m)}) + s_{j-1/2}^+s_{j-1/2}^-(\alpha_j^{(m)} - \alpha_{j-1}^{(m)})]}{s_{j-1/2}^+ - s_{j-1/2}^-}\Big]\Big\}, \\
\alpha_j^{(l)} = \alpha_j^{**} - a_{l,l}\frac{\Delta t}{2\Delta x}(1-\epsilon)u_j^{**}(\alpha_{j+1}^{**} - \alpha_{j-1}^{**}).
\end{cases} \tag{87}$$

Eq. (86) (or (87)) gives also the value α^* introduced in sect. 3.2 that must be used to obtain a well-balanced scheme. In other words, with the particular linearizations introduced in sect. 3.2 and given the numerical flux function (either Rusanov, or HLL), the only way to obtain a well-balanced scheme is to use the value α^*, discretize non-conservative terms using (78) (or (79)), and update the volumetric fraction according to (86) (or (87)). With the discretizations introduced for all the non conservative terms is easy to verify that also the pressure correction equations (56) and (55) preserve the steady state solution in the sense that pressure and velocity remain constant.

4.3. Numerical scheme structure

To summarize, we now present the main steps required to update the solution of eqs. (1) from time t^n to t^{n+1}.

Assuming that the solution vector of conservative variables at time step t^n is known, the all-Mach numerical scheme boils down to the following steps.

1. Using the solution of the previous time step, U^n, for each stage of the Runge-Kutta method, $l = 1, \dots, s$
   (a) Compute $(\alpha\rho)_k^{(l)}$ using eq. (45) and Rusanov (or HLL) fluxes for the explicit part of the convective term.
   (b) Compute the *prediction* for momentum and energy, $(\alpha\rho u)_k^*$ and $(\alpha\rho E)_k^*$ using eq. (47) and the well balanced discretization of non-conservative terms (78) (or (79), depending on the numerical flux function).
   (c) Compute a *prediction* for volumetric fractions, α_k^*, using the first eq. in (86) (or (87), depending on the numerical flux function).
   (d) *Velocity relaxation*. Compute the solution of the velocity relaxation step by solving the system of ODEs (51).
   (e) *Pressure relaxation*. Using the solution of the velocity relaxation, solve the system of ODEs (52). In the special case of instantaneous pressure relaxation, this amounts to solving the system of non-linear equations (58).
   (f) Solve the system of non-linear elliptic equations for phasic pressures (57) (or a single equation (59) in case of instantaneous pressure relaxation).
   (g) *Correct* the prediction for momentum using eq. (56) (or (62) in case of instantaneous velocity relaxation) to compute $(\alpha\rho u)_k^{(l)}$ and for energy using eq. (55) to compute $(\alpha\rho E)_k^{(l)}$.
   (h) Update volumetric fraction $\alpha_k^{(l)}$ using the second eq. in (86) (or (87) depending on the numerical flux function).
2. Update the solution using equation (63).

5. Asymptotic preserving property

In this section, we prove that our numerical scheme is asymptotic preserving (AP) in the sense that we recover the correct asymptotic limit also at the discrete level in the limit $M \to 0$. Formally, let $\mathcal{S}^M$ be the continuous Baer-Nunziato model, which depends on the Mach number M, and let $\mathcal{S}^0$ be the continuous model obtained in the limit $M \to 0$. Let $\mathcal{S}_\Delta^M$ be a consistent discretization of $\mathcal{S}^M$ with discretization parameters $\Delta := (\Delta x, \Delta t)$. The scheme $\mathcal{S}_\Delta^M$ is asymptotic preserving if its stability condition is independent of M and the limiting discrete model $\mathcal{S}_\Delta^0$ is consistent with $\mathcal{S}^0$.

$$\begin{array}{ccc}
\mathcal{S}_\Delta^M & \xrightarrow{M\to 0} & \mathcal{S}_\Delta^0 \\
\downarrow{\scriptstyle \Delta\to 0} & & \downarrow{\scriptstyle \Delta\to 0} \\
\mathcal{S}^M & \xrightarrow{M\to 0} & \mathcal{S}^0
\end{array}$$

In order to prove the AP property, there are three steps to follow.

- First, we derive the continuous model in the asymptotic limit, that is $\mathcal{S}^M \xrightarrow{M\to 0} \mathcal{S}^0$. This was presented in subsection 2.3,
- Second, we derive the limit of the discrete scheme $\mathcal{S}_\Delta^M \xrightarrow{M\to 0} \mathcal{S}_\Delta^0$,
- Third, we show that $\mathcal{S}_\Delta^0$ is a consistent discretization of $\mathcal{S}^0$.

5.1. Asymptotic analysis of the numerical scheme

We start noticing that the numerical flux functions used throughout this work are a consistent discretization of the continuous flux function, i.e. $\mathcal{F}(U,U) = F(U)$ for any U. Furthermore, it is easy to show that discretizations of space derivative used in the elliptic pressure equation and in the stiff part of the convective fluxes are also consistent in the limit $\Delta x \to 0$. Therefore, we only need to prove the AP property for the semi-discrete model. To this end, we derive the limit for $M \to 0$ of the semi-discrete system $\mathcal{S}_{\Delta}^{M}$ assuming that the IMEX Runge-Kutta scheme is consistent with the model equations in the limit $\Delta t \to 0$. This holds true if the usual conditions on the Butcher's tableau are fulfilled (see for instance [22]). As done in subsection 2.3, we consider first the case where both phases are in the same Mach regime ($M_1 = M_2 = M$), then the case of one compressible ($M_1 = O(1)$) and one weakly compressible ($M_2 \ll 1$) phase.

Case 1 We assume the initial data at time t^n is well-prepared in the sense defined in subsection 2.3 (case 1). Next, we expand discrete variables with respect to the common Mach number $M_1 = M_2 = M$, that is:

$$\begin{aligned}
&\rho_k = \rho_{k,0} + M\rho_{k,1} + M^2\rho_{k,2},\\
&u_k = u_{k,0} + Mu_{k,1} + M^2u_{k,2},\\
&u_I = u_{I,0} + Mu_{I,1} + M^2u_{I,2}, \quad u_{k,0} = u_{I,0} = u_0, \quad \partial_x u_0 = 0,\\
&p_k = p_{k,0} + Mp_{k,1} + M^2p_{k,2},\\
&p_I = p_{I,0} + Mp_{I,1} + M^2p_{I,2}, \quad p_{k,0} = p_0, \quad p_{k,1} = p_1,\\
&\alpha_k = \alpha_{k,0} + O(M)
\end{aligned} \tag{88}$$

We start the analysis from the implicit step of an intermediate stage l of the RK method and consider the non-dimensional relaxations systems for phase k. Given the vector of conserved variables at the previous time step, U^n, at the first stage of the IMEX-RK scheme we have $U^* = U^n$. Regarding pressure relaxation (equation (52)), we denote with $(\cdot)^{(pr)}$ the state after the relaxation procedure. We see that at order $O(1/M^2)$ we have $p_{1,0}^{(pr)} = p_{2,0}^{(pr)}$ and similarly at order $O(1/M)$ we have $p_{1,1}^{(pr)} = p_{2,1}^{(pr)}$; both in accordance with the well-prepared initial data. Finally at order $O(1)$ equations read:

$$\begin{cases}
(\alpha\rho)_{k,0}^{(pr)} = (\alpha\rho)_{k,0}^{*}\\
(\alpha\rho u)_{k,0}^{(pr)} = (\alpha\rho u)_{k,0}^{*}\\
(\alpha\rho e)_{k,0}^{(pr)} = (\alpha\rho e)_{k,0}^{*} - \Delta t a_{l,l}\nu_{k,j}p_{I,0}^{(pr)}(p_{k,2}^{(pr)} - p_{j,2}^{(pr)})\\
\alpha_{k,0}^{(pr)} = \alpha_{k,0}^{*} + \Delta t a_{l,l}\nu_{k,j}(p_{k,2}^{(pr)} - p_{j,2}^{(pr)})
\end{cases} \tag{89}$$

from which we see that the velocity does not change at any order through this step ($u_k^{(pr)} = u_k^*$).

Moving to the velocity relaxation step (equation (51)), using values at state $(\cdot)^{(pr)}$ as input and denoting as $(\cdot)^{(vr)}$ the state after homogenization of velocities, we can write the system at order $O(1)$:

$$\begin{cases}
(\alpha\rho)_k^{(vr)} = (\alpha\rho)_k^{(pr)}\\
(\alpha\rho u)_k^{(vr)} = (\alpha\rho u)_k^{(pr)} + \Delta t a_{l,l}\tau_{k,j}(u_{k,0}^{(vr)} - u_{j,0}^{(vr)})\\
(\alpha\rho K)_k^{(vr)} = (\alpha\rho K)_k^{(pr)} + \Delta t a_{l,l}\tau_{k,j}u_{I,0}^{(vr)}(u_{k,0}^{(vr)} - u_{j,0}^{(vr)})\\
\alpha_k^{(vr)} = \alpha_k^{(pr)},
\end{cases} \tag{90}$$

where form the momentum equation we have:

$$u_k^{(vr)} = u_k^{(pr)} + \Delta t a_{l,l}\tau_{k,j}(u_{k,0}^{(vr)} - u_{j,0}^{(vr)})/(\alpha\rho)_k^{(pr)} \tag{91}$$

therefore, we have $u_k^{(vr)} = u_k^{(pr)} + O(\Delta t)$ and consequently $\partial_x u_k^{(vr)} = O(\Delta t)$.

Being U^{**} the state after both relaxations we now consider the non-dimensional elliptic pressure equation written for phase k at an intermediate stage l of the RK method:

$$\begin{aligned}
&(\alpha\rho e)_k^{(l)} + \frac{1}{2}\chi u_k^{**}\left(-\partial_x(\alpha p)_k^{(l)} + p_I^{(l)}\partial_x\alpha_k^{(l)}\right) - \chi u_I^{**}p_I^{(l)}\partial_x\alpha_k^{**}\\
&\quad + \chi^2\partial_x\left[H_k^{**}\left(-\frac{1}{M^2}\partial_x(\alpha p)_k^{(l)} + \frac{1}{M^2}p_I^{(l)}\partial_x\alpha_k^{(l)}\right)\right] =\\
&\quad (\alpha\rho e)_k^{**} - \chi\,\partial_x\left((\alpha\rho u)_k^{**}H_k^{**}\right).
\end{aligned} \tag{92}$$

Expanding all variables we obtain (at order $O(1/M^2)$):

$$\partial_x(\alpha_{k,0}p_0)^{(l)} = p_{I,0}^{(l)}\partial_x\alpha_{k,0}^{(l)} \tag{93}$$

and at order $O(1/M)$:

$$\partial_x(\alpha_{k,0}p_1)^{(l)} = p_{I,1}^{(l)}\partial_x\alpha_{k,0}^{(l)}. \tag{94}$$

Following the same step of sect. 2.3, adding eqs. (93) written for each phase gives:

$$\partial_x(p_0^{(l)}(\alpha_{1,0}^{(l)} + \alpha_{2,0}^{(l)})) = p_{I,0}^{(l)}\partial_x(\alpha_{1,0}^{(l)} + \alpha_{2,0}^{(l)}) \tag{95}$$

which implies $\partial_x p_0^{(l)} = 0$ because as for the derivation of the low-Mach limit we assume $\alpha_{1,0}^{(l)} + \alpha_{2,0}^{(l)} = 1$ so that $\partial_x(\alpha_{1,0}^{(l)} + \alpha_{2,0}^{(l)}) = 0$. Similarly, subtracting eqs (93) written for each phase and using the fact that $\partial_x p_0^{(l)} = 0$ leads to $p_{I,0}^{(l)} = p_0^{(l)}$. By repeating the same algebraic manipulations for terms at order $O(1/M)$, we obtain $\partial_x p_1^{(l)} = 0$ and $p_{I,1}^{(l)} = p_1^{(l)}$. From these, we deduce that pressure is constant in space up to fluctuations of order M^2 at each intermediate stage of the RK method. We now analyze the corrector step and the equation used to update volumetric fractions:

$$\begin{cases}
(\alpha\rho)_k^{(l)} = (\alpha\rho)_k^{**}\\
(\alpha\rho u)_k^{(l)} = (\alpha\rho u)_k^{**} + \Delta t a_{l,l}\frac{1-M^2}{M^2}\left[-\partial_x(\alpha p)_k^{(l)} + \left(p_I\partial_x\alpha_k\right)^{(l)}\right]\\
(\alpha\rho E)_k^{(l)} = (\alpha\rho E)_k^{**} + \Delta t a_{l,l}\frac{1-M^2}{M^2}\left[-\partial_x\left(H_k^{**}(\alpha\rho u)_k^{(l)}\right)\right.\\
\qquad\qquad \left. + \left(p_I^{(l)}u_I^{**}\partial_x\alpha_k^{**}\right)\right]\\
\alpha_k^{(l)} = \alpha_k^{**} - \Delta t a_{l,l}(1-M^2)(u_I\partial_x\alpha_k)^{**}
\end{cases} \tag{96}$$

Expanding each variable and using previous results in momentum equation, we obtain at order $O(1/M^2)$:

$$\partial_x(\alpha_{k,0}p_0)^{(l)} = p_0^{(l)}\partial_x\alpha_{k,0}^{(l)} \tag{97}$$

and at order $O(1/M)$:

$$\partial_x(\alpha_{k,0}p_1)^{(l)} = p_1^{(l)}\partial_x\alpha_{k,0}^{(l)}, \tag{98}$$

which are trivially satisfied because $\partial_x p_0^{(l)} = 0$ and $\partial_x p_1^{(l)} = 0$. Finally, expanding variables in (96), we obtain at the 0^{th} order:

$$\begin{cases}
(\alpha_{k,0}\rho_{k,0})^{(l)} = (\alpha_{k,0}\rho_{k,0})^{**}\\
(\alpha_{k,0}\rho_{k,0}u_0)^{(l)} = (\alpha_{k,0}\rho_{k,0}u_0)^{**} - \Delta t a_{l,l}\partial_x\left(\alpha_{k,0}p_{k,2}\right)^{(l)}\\
\qquad\qquad + \Delta t a_{l,l}(p_{I,2}\partial_x\alpha_{k,0})^{(l)}\\
(\alpha_{k,0}\rho_{k,0}e_{k,0})^{(l)} = (\alpha_{k,0}\rho_{k,0}e_{k,0})^{**} - \Delta t a_{l,l}\partial_x\left(H_{k,0}^{**}\left(\alpha_{k,0}\rho_{k,0}u_{k,0}\right)^{(l)}\right)\\
\qquad\qquad + \Delta t a_{l,l}(p_0^{(l)}u_0^{**}\partial_x\alpha_{k,0}^{**})\\
\alpha_{k,0}^{(l)} = \alpha_{k,0}^{**} - \Delta t a_{l,l}(u_0\partial_x\alpha_{k,0})^{**}
\end{cases} \tag{99}$$

We now use the state law $p_k = (\gamma - 1)(\rho_k e_k)$ and expand the internal energy as follows:

$$e_k = \frac{p_0}{\rho_{k,0}} + M\left(\frac{p_1}{\beta_k\rho_{k,0}} + \frac{p_{k,2}}{\beta_k\rho_{k,1}}\right) + O(M^2). \tag{100}$$

Subtracting the volume fraction equation in eq. (99) multiplied by $p_0^{(l)}$ from the energy equation and assuming well-prepared initial data, we obtain that $u_0^{(l)} = u_0^{**}$. From previous relations thus we have $\partial_x u_0^{(l)} = O(\Delta t)$.

To summarize, the asymptotic limit of the implicit step is:

$$\begin{cases} \partial_x p_0^{(l)} = 0 \\ \partial_x p_1^{(l)} = 0 \\ (\alpha_{k,0}\rho_{k,0})^{(l)} = (\alpha_{k,0}\rho_{k,0})^{**} \\ (\alpha_{k,0}\rho_{k,0}u_0)^{(l)} = (\alpha_{k,0}\rho_{k,0}u_0)^{**} - \Delta t a_{l,l}\partial_x\left(\alpha_{k,0}p_{k,2}\right)^{(l)} \\ \qquad\qquad + \Delta t a_{l,l}(p_{I,2}\partial_x\alpha_{k,0})^{(l)} \\ \partial_x u_0^{(l)} = O(\Delta t) \\ \alpha_{k,0}^{(l)} = \alpha_{k,0}^{**} - \Delta t a_{l,l}(u_0\partial_x\alpha_0)^{**} \end{cases} \tag{101}$$

which shows that pressure is constant in space up to fluctuations of order M^2 and the velocity field is divergence-free in the limit $\Delta t \to 0$ at each stage of the IMEX-RK method.

We now analyze the explicit part of the numerical scheme.

The explicit part of the scheme for phase k at stage i reads as follows in non-dimensional form:

$$\begin{cases} (\alpha\rho)_k^{(i)} = (\alpha\rho)_k^{(i-1)} - \Delta t\tilde{a}_{l,i-1}\partial_x(\alpha\rho u)_k^{(i-1)} \\ (\alpha\rho u)_k^{(i)} = (\alpha\rho u)_k^{(i-1)} - \Delta t\tilde{a}_{l,i-1}\partial_x\left[(\alpha\rho uu)_k^{(i-1)} + (\alpha p)_k^{(i-1)}\right] \\ \qquad + \Delta t\tilde{a}_{l,i-1}\left(p_I\partial_x\alpha_k\right)^{(i-1)} \\ (\alpha\rho E)_k^{(i)} = (\alpha\rho E)_k^{(i-1)} \\ \qquad - \Delta t\tilde{a}_{l,i-1}\partial_x\left[M^2(u\alpha\rho K)_k^{(i-1)} + M^2\left((u\alpha\rho e)_k^{(i-1)} + (u\alpha p)_k^{(i-1)}\right)\right] \\ \qquad + \Delta t\tilde{a}_{l,i-1}M^2\left(p_I u_I\partial_x\alpha_k\right)^{(i-1)} \\ \alpha_k^{(i)} = \alpha_k^{(i-1)} - \Delta t\tilde{a}_{l,i-1}M^2(u_I\partial_x\alpha_k)^{(i-1)} \end{cases} \tag{102}$$

where $E_k = e_k + 1/2M^2u_k^2$. Substituting the asymptotic expansion of each variable and using (101), we find (order $O(1)$):

$$\begin{cases} (\alpha_{k,0}\rho_{k,0})^{(i)} = (\alpha_{k,0}\rho_{k,0})^{(i-1)} - \Delta t\tilde{a}_{l,i-1}u_0^{(i-1)}\partial_x\left(\alpha_{k,0}\rho_{k,0}\right)^{(i-1)} \\ (\alpha_{k,0}\rho_{k,0}u_0)^{(i)} = (\alpha_{k,0}\rho_{k,0}u_0)^{(i-1)} - \Delta t\tilde{a}_{l,i-1}u_0^{(i-1)}\partial_x\left(\alpha_{k,0}\rho_{k,0}u_0\right)^{(i-1)} \\ (\alpha_{k,0}\rho_{k,0}e_{k,0})^{(i)} = (\alpha_{k,0}\rho_{k,0}e_{k,0})^{(i-1)} \\ \alpha_{k,0}^{(i)} = \alpha_{k,0}^{(i-1)}, \end{cases} \tag{103}$$

which shows that (at the 0^{th} order) volumetric fraction remains constant. From the energy equation we deduce that also the leading term of pressure remains unchanged as obtained for the continuous case. Since both spatial and temporal discretization are consistent, it follows that our numerical scheme is consistent with model equations in the limits $M \to 0$ and $\Delta t \to 0$. Thus, we conclude that our scheme is AP.

Case 2 We assume that $M_1 = 1$ and $M_2 \ll 1$. Let the initial data at time t^n be well-prepared ($\psi \in \Psi_{c-i}^{wp}$). We have for the compressible phase $\rho_1 = \rho_{1,0} + O(M_2)$, $u_1 = u_{1,0} + O(M_2)$ and $p_1 = p_{1,0} + O(M_2)$. The other variables are expanded as follows:

$$\begin{aligned} &\alpha_1 = \alpha_{1,0} + M_2\alpha_{1,1} + M_2^2\alpha_{1,2}, \\ &\rho_2 = \rho_{2,0} + M_2\rho_{2,1} + M_2^2\rho_{2,2}, \\ &u_2 = u_{2,0} + M_2u_{2,1} + M_2^2u_{2,2}, \quad \partial_x u_{2,0} = 0, \quad u_{2,0} = u_{1,0} \\ &p_2 = M_2^2 p_{2,2}, \\ &\alpha_2 = \alpha_{2,0} + M_2\alpha_{2,1} + M_2^2\alpha_{2,2}, \\ &u_I = u_{I,0} + M_2u_{I,1} + M_2^2u_{I,2}. \end{aligned} \tag{104}$$

Given that $p_I = \alpha_1 p_1 + \alpha_2 p_2$, and assuming well-prepared initial data, the interface pressure p_I is expanded as:

$$\begin{aligned} p_I &= \alpha_{1,0}p_{1,0} + M_2\alpha_{1,1}p_{1,0} + M_2^2(\alpha_{2,0}p_{2,2} + \alpha_{1,2}p_{1,0}) \\ &= p_{I,0} + M_2p_{I,1} + M_2^2p_{I,2}. \end{aligned} \tag{105}$$

We start again the analysis from the implicit step of a generic stage l of the RK method. At the first stage of the scheme, we have $U^* = U^n$. As done for *case 1*, we begin considering the pressure relaxation operator (equation (52)). Denoting $(\cdot)^{(pr)}$ the state after pressure relaxation, we have from the volume fraction equations that at order $O(1/M_2^2)$ we obtain $p_{2,0}^{(pr)} = 0$ and similarly from order $O(1/M_2)$ terms $p_{2,1}^{(pr)} = 0$, in accordance with the well-prepared initial data. Finally, at order $O(1)$:

$$\begin{cases} (\alpha\rho)_1^{(pr)} = (\alpha\rho)_1^* \\ (\alpha\rho u)_1^{(pr)} = (\alpha\rho u)_1^* \\ (\alpha\rho E)_1^{(pr)} = (\alpha\rho E)_1^* - \Delta t a_{l,l}\nu_{1,2}p_{I,0}^{(pr)}(p_{1,0}^{(pr)} - p_{2,2}^{(pr)}) \\ \alpha_1^{(pr)} = \alpha_1^* + \Delta t a_{l,l}\nu_{1,2}(p_{1,0}^{(pr)} - p_{2,2}^{(pr)}) \\ (\alpha\rho)_2^{(pr)} = (\alpha\rho)_2^* \\ (\alpha\rho u)_2^{(pr)} = (\alpha\rho u)_2^* \\ (\alpha\rho e)_2^{(pr)} = (\alpha\rho e)_2^* - \Delta t a_{l,l}\nu_{2,1}p_{I,0}^{(pr)}(p_{2,2}^{(pr)} - p_{1,0}^{(pr)}) \\ \alpha_2^{(pr)} = \alpha_2^* + \Delta t a_{l,l}\nu_{2,1}(p_{2,2}^{(pr)} - p_{1,0}^{(pr)}). \end{cases} \tag{106}$$

We note that velocities do not change at any order through this step, consequently $u_k^{(pr)} = u_k^*$ which implies $\partial_x u_{2,0}^{(pr)} = \partial_x u_{2,0}^* = 0$. Looking now at the velocity relaxation, denoting with $(\cdot)^{(vr)}$ the state after the homogenization of the velocities, we write the system at order $O(1)$:

$$\begin{cases} (\alpha\rho)_1^{(vr)} = (\alpha\rho)_1^{(pr)} \\ (\alpha\rho u)_1^{(vr)} = (\alpha\rho u)_1^{(pr)} + \Delta t a_{l,l}\tau_{1,2}(u_{1,0}^{(vr)} - u_{2,0}^{(vr)}) \\ (\alpha\rho E)_1^{(vr)} = (\alpha\rho E)_1^{(pr)} + \Delta t a_{l,l}\tau_{1,2}u_{I,0}^{(vr)}(u_{1,0}^{(vr)} - u_{2,0}^{(vr)}) \\ \alpha_1^{(vr)} = \alpha_1^{(pr)} \\ (\alpha\rho)_2^{(vr)} = (\alpha\rho)_2^{(pr)} \\ (\alpha\rho u)_2^{(vr)} = (\alpha\rho u)_2^{(pr)} + \Delta t a_{l,l}\tau_{2,1}(u_{2,0}^{(vr)} - u_{1,0}^{(vr)}) \\ (\alpha\rho K)_2^{(vr)} = (\alpha\rho K)_2^{(pr)} + \Delta t a_{l,l}\tau_{2,1}u_{I,0}^{(vr)}(u_{2,0}^{(vr)} - u_{1,0}^{(vr)}) \\ \alpha_2^{(vr)} = \alpha_2^{(pr)}. \end{cases} \tag{107}$$

We note from the momentum equation for phase 2 that $u_{2,0}^{(vr)} = u_{2,0}^{(pr)} + O(\Delta t)$ thus $\partial_x u_{2,0}^{(vr)} = O(\Delta t)$.

As done for *case 1*, being U^{**} the variables after both relaxations, we consider the non-dimensional pressure equation (92) for a generic stage l of the RK method. The pressure equation written for phase 1 is:

$$\begin{aligned} &(\alpha\rho e)_1^{(l)} + \frac{1}{2}\chi u_1^{**}\left(-\partial_x(\alpha p)_1^{(l)} + p_I^{(l)}\partial_x\alpha_1^{(l)}\right) - \chi u_I^{**}p_I^{(l)}\partial_x\alpha_1^{**} \\ &\qquad + \chi^2\partial_x\left[H_1^{**}\left(-\partial_x(\alpha p)_1^{(l)} + p_I^{(l)}\partial_x\alpha_1^{(l)}\right)\right] = \\ &\qquad (\alpha\rho e)_1^{**} - \chi\partial_x\left((\alpha\rho u)_1^{**}H_1^{**}\right) \end{aligned} \tag{108}$$

which holds true at any order of the expansion since all terms are in the same order of magnitude.

Equation (92) written for phase 2 is:

$$\begin{aligned} &(\alpha\rho e)_2^{(l)} + \frac{1}{2}\chi u_2^{**}\left(-\partial_x(\alpha p)_2^{(l)} + p_I^{(l)}\partial_x\alpha_2^{(l)}\right) - \chi u_I^{**}p_I^{(l)}\partial_x\alpha_2^{**} \\ &\qquad + \chi^2\partial_x\left[H_2^{**}\left(-\frac{1}{M_2^2}\partial_x(\alpha p)_2^{(l)} + \frac{1}{M_2^2}p_I^{(l)}\partial_x\alpha_2^{(l)}\right)\right] = \\ &\qquad (\alpha\rho e)_2^{**} - \chi\partial_x\left((\alpha\rho u)_2^{**}H_2^{**}\right). \end{aligned} \tag{109}$$

Expanding variables as in (104), we obtain:

$$\begin{aligned} O(1/M_2^2) \quad &: \quad 0 = p_{I,0}^{(l)}\partial_x\alpha_{2,0}^{(l)} \\ O(1/M_2) \quad &: \quad 0 = p_{I,1}^{(l)}\partial_x\alpha_{2,0}^{(l)} + p_{I,0}^{(l)}\partial_x\alpha_{2,1}^{(l)} \end{aligned} \tag{110}$$

We are interested in regions where both phases are present, so we assume $\alpha_{1,0}^{(l)} \neq 0$ and $p_{1,0}^{(l)}(x,t) \neq 0$. Using the fact that $p_{I,0}^{(l)} = \alpha_{1,0}^{(l)}p_{1,0}^{(l)}$, (110) gives $\partial_x\alpha_{2,0}^{(l)} = 0$ at order $O(1/M_2^2)$. The same argument can be applied to terms of order $O(1/M_2)$ to obtain $\partial_x\alpha_{2,1}^{(l)} = 0$.

With these results, we now analyze the corrector step for both phases:

$$\begin{cases}(\alpha\rho)_1^{(l)} = (\alpha\rho)_1^{**}\\ (\alpha\rho u)_1^{(l)} = (\alpha\rho u)_1^{**} + \Delta t a_{l,l}\frac{1-M_1^2}{M_1^2}\left[-\partial_x(\alpha p)_1^{(l)} + \left(p_I\partial_x\alpha_1\right)^{(l)}\right]\\ (\alpha\rho E)_1^{(l)} = (\alpha\rho E)_1^{**} + \Delta t a_{l,l}\dfrac{1-M_1^2}{M_1^2}\Big[-\partial_x\left(H_1^{**}(\alpha\rho u)_1^{(l)}\right)\\ \qquad + \left(p_I^{(l)}u_I^{**}\partial_x\alpha_1^{**}\right)\Big]\\ \alpha_1^{(l)} = \alpha_1^{**} - \Delta t a_{l,l}(1-M_1^2)(u_I\partial_x\alpha_1)^{**}\\ (\alpha\rho)_2^{(l)} = (\alpha\rho)_2^{**}\\ (\alpha\rho u)_2^{(l)} = (\alpha\rho u)_2^{**} + \Delta t a_{l,l}\frac{1-M_1^2}{M_2^2}\left[-\partial_x(\alpha p)_2^{(l)} + \left(p_I\partial_x\alpha_2\right)^{(l)}\right]\\ (\alpha\rho E)_2^{(l)} = (\alpha\rho E)_2^{**} + \Delta t a_{l,l}\dfrac{1-M_1^2}{M_2^2}\Big[-\partial_x\left(H_2^{**}(\alpha\rho u)_2^{(l)}\right)\\ \qquad + \left(p_I^{(l)}u_I^{**}\partial_x\alpha_2^{**}\right)\Big]\\ \alpha_2^{(l)} = \alpha_2^{**} - \Delta t a_{l,l}(1-M_1^2)(u_I\partial_x\alpha_2)^{**}.\end{cases} \tag{111}$$

Since $M_1 = 1$ and since the splitting is based on the Mach number of the most compressible phase, we have that all the conserved quantities remain unchanged during the corrector step at the 0^{th} order. Furthermore, momentum equation for phase 2 gives (at order $O(1)$) $u_{2,0}^{**} = u_{2,0}^{(l)}$, which implies $\partial_x u_{2,0}^{**} = \partial_x u_{2,0}^{(l)} = O(\Delta t)$. From the energy equation written for phase 2, we obtain $p_2^{**} = p_2^{(l)}$ which implies $p_2^{(l)} = M_2^2 p_{2,2}^{(l)}$, that is the solution at stage l is a well-prepared initial datum for the next stage of the RK method.

To summarize, at the end of the implicit step of our scheme, we have:

$$\begin{cases}(\alpha_{1,0}\rho_{1,0})^{(l)} = (\alpha_{1,0}\rho_{1,0})^{**}\\ (\alpha_{1,0}\rho_{1,0}u_{1,0})^{(l)} = (\alpha_{1,0}\rho_{1,0}u_{1,0})^{**}\\ (\alpha_{1,0}\rho_{1,0}E_{1,0})^{(l)} = (\alpha_{1,0}\rho_{1,0}E_{1,0})^{**}\\ \alpha_{1,0}^{(l)} = \alpha_{1,0}^{**}\\ (\alpha_{2,0}\rho_{2,0})^{(l)} = (\alpha_{2,0}\rho_{2,0})^{**}\\ (\alpha_{2,0}\rho_{2,0}u_{2,0})^{(l)} = (\alpha_{2,0}\rho_{2,0}u_{2,0})_2^{**}\\ \alpha_{2,0}^{(l)} = \alpha_{2,0}^{**}\\ \partial_x u_{2,0}^{(l)} = \partial_x u_{2,0}^{**} = O(\Delta t)\\ p_2^{(l)} = M_2^2 p_{2,2}^{(l)}.\end{cases} \tag{112}$$

We now analyze the explicit part of the scheme for phase 1. Using previous results, at order $O(1)$ we obtain:

$$\begin{cases}(\alpha_{1,0}\rho_{1,0})^{(i)} = (\alpha_{1,0}\rho_{1,0})^{(i-1)} - \Delta t\tilde{a}_{l,i-1}\partial_x\left(\alpha_{1,0}\rho_{1,0}u_{1,0}\right)^{(i-1)}\\ (\alpha_{1,0}\rho_{1,0}u_{1,0})^{(i)} = (\alpha_{1,0}\rho_{1,0}u_{1,0})^{(i-1)}\\ \qquad - \Delta t\tilde{a}_{l,i-1}\partial_x\left[\left(\alpha_{1,0}\rho_{1,0}u_{1,0}u_{1,0}\right)^{(i-1)} + \left(\alpha_{1,0}p_{1,0}\right)^{(i-1)}\right]\\ \qquad + \Delta t\tilde{a}_{l,i-1}\left(p_{I,0}\partial_x\alpha_{1,0}\right)^{(i-1)}\\ (\alpha_{1,0}\rho_{1,0}E_{1,0})^{(i)} = (\alpha_{1,0}\rho_{1,0}E_{1,0})^{(i-1)} - \Delta t\tilde{a}_{l,i-1}\partial_x\left(u_{1,0}\alpha_{1,0}\rho_{1,0}K_{1,0}\right)^{(i-1)}\\ \qquad - \Delta t\tilde{a}_{l,i-1}\partial_x\Big(\left(u_{1,0}\alpha_{1,0}\rho_{1,0}e_{1,0}\right)^{(i-1)}\\ \qquad + \left(u_{1,0}\alpha_{1,0}p_{1,0}\right)^{(i-1)}\Big)\\ \qquad + \Delta t\tilde{a}_{l,i-1}\left(p_{I,0}u_{I,0}\partial_x\alpha_{1,0}\right)^{(i-1)}\\ \alpha_{1,0}^{(i)} = \alpha_{1,0}^{(i-1)} - \Delta t\tilde{a}_{l,i-1}(u_{I,0}\partial_x\alpha_{1,0})^{(i-1)}.\end{cases} \tag{113}$$

For phase 1, all the terms appearing in the above equations are in the same order of magnitude, while the explicit part of the numerical scheme written for phase 2 becomes:

$$\begin{cases}(\alpha\rho)_2^{(i)} = (\alpha\rho)_2^{(i-1)} - \Delta t\tilde{a}_{l,i-1}\partial_x(\alpha\rho u)_2^{(i-1)}\\ (\alpha\rho u)_2^{(i)} = (\alpha\rho u)_2^{(i-1)} - \Delta t\tilde{a}_{l,i-1}\partial_x\left[(\alpha\rho uu)_2^{(i-1)} + \dfrac{1}{M_2^2}(\alpha p)_2^{(i-1)}\right]\\ \qquad + \Delta t\tilde{a}_{l,i-1}\left(\dfrac{1}{M_2^2}p_I\partial_x\alpha_2\right)^{(i-1)}\\ (\alpha\rho E)_2^{(i)} = (\alpha\rho E)_2^{(i-1)}\\ \qquad - \Delta t\tilde{a}_{l,i-1}\partial_x\left[M_2^2(u\alpha\rho K)_2^{(i-1)} + (u\alpha\rho e)_2^{(i-1)} + (u\alpha p)_2^{(i-1)}\right]\\ \qquad + \Delta t\tilde{a}_{l,i-1}\left(p_I u_I\partial_x\alpha_2\right)^{(i-1)}\\ \alpha_2^{(i)} = \alpha_2^{(i-1)} - \Delta t\tilde{a}_{l,i-1}M^2(u_I\partial_x\alpha_2)^{(i-1)}\end{cases} \tag{114}$$

where $E_k = e_k + 1/2M_2^2u_k^2$. Expanding variables and using the results obtained from the implicit part of the scheme in the momentum equation, we get:

$$\begin{aligned}O(1/M_2^2) \quad &: \quad 0 = p_{I,0}^{(i-1)}\partial_x\alpha_{2,0}^{(i-1)}\\ O(1/M_2) \quad &: \quad 0 = p_{I,1}^{(i-1)}\partial_x\alpha_{2,0}^{(i-1)} + p_{I,0}^{(i-1)}\partial_x\alpha_{2,1}^{(i-1)}\end{aligned} \tag{115}$$

Both equalities are satisfied since we already obtained $\partial_x\alpha_{2,0}^{(i-1)} = \partial_x\alpha_{2,0}^{(l)} = 0$ and $\partial_x\alpha_{2,1}^{(i-1)} = \partial_x\alpha_{2,1}^{(l)} = 0$ from the implicit step. Next, from the energy equation (at order $O(1)$), we get:

$$\begin{aligned}(\alpha_{2,0}\rho_{2,0}e_{2,0})^{(i)} = (\alpha_{2,0}\rho_{2,0}e_{2,0})^{(i-1)}\\ - \Delta t\tilde{a}_{l,i-1}\partial_x\left(\left(u_{2,0}\alpha_{2,0}\rho_{2,0}e_{2,0}\right)^{(i-1)} + \left(u_{2,0}\alpha_{2,0}p_{2,0}\right)^{(i-1)}\right)\\ + \Delta t\tilde{a}_{l,i-1}\left(p_{I,0}u_{I,0}\partial_x\alpha_{2,0}\right)^{(i-1)},\end{aligned} \tag{116}$$

where non-conservative terms vanish because $\partial_x\alpha_{2,0}^{(i-1)} = \partial_x\alpha_{2,0}^{(l)} = 0$. From the implicit step we also have that pressure for the weakly compressible phase is given by $p_2^{(i-1)} = M_2^2 p_{2,2}^{(i-1)}$, therefore at the 0^{th} order, $p_{2,0}^{(i-1)} = 0$. As discussed in subsection 2.3, this means that the 0^{th} order solution for phase 2 is approaching a near-vacuum state. Using again the stiffened gas EOS for phase 2 in place of the perfect gas EOS, internal energy can be expanded as follows:

$$e_2 = \frac{\eta_2}{\beta_2\rho_{2,0}} + O(M_2). \tag{117}$$

After expanding all the variables in eq. (116), we obtain:

$$\frac{\eta_2}{\beta_2}\alpha_{2,0}^{(i)} = \frac{\eta_2}{\beta_2}\alpha_{2,0}^{(i-1)} - \Delta t\tilde{a}_{l,i-1}\frac{\eta_2}{\beta_2}\alpha_{2,0}^{(i-1)}\partial_x u_{2,0}^{(i-1)} \tag{118}$$

From this, assuming periodic (or fixed) boundary conditions, we obtain the asymptotic limit for the explicit part of our scheme for the weakly compressible phase:

$$\begin{cases}(\alpha_{2,0}\rho_{2,0})^{(i)} = (\alpha_{2,0}\rho_{2,0})^{(i-1)} - \Delta t\tilde{a}_{l,i-1}\alpha_{2,0}^{(i-1)}u_{2,0}^{(i-1)}\partial_x\rho_{2,0}^{(i-1)}\\ (\alpha_{2,0}\rho_{2,0}u_{2,0})^{(i)} = (\alpha_{2,0}\rho_{2,0}u_{2,0})^{(i-1)} - \Delta t\tilde{a}_{l,i-1}\alpha_{2,0}^{(i-1)}u_{2,0}^{(i-1)}\partial_x\left(\rho_{2,0}u_{2,0}\right)^{(i-1)}\\ \qquad - \Delta t\tilde{a}_{l,i-1}\alpha_{2,0}^{(i-1)}\partial_x p_{2,2}^{(i-1)}\\ \qquad + \Delta t\tilde{a}_{l,i-1}p_{I,0}^{(i-1)}\partial_x\alpha_{2,2}^{(i-1)}\\ \alpha_{2,0}^{(i)} = \alpha_{2,0}^{(i-1)} - \Delta t\tilde{a}_{l,i-1}u_{I,0}^{(i-1)}\partial_x\alpha_{2,0}^{(i-1)}\\ \partial_x u_{2,0}^{(i-1)} = O(\Delta t).\end{cases} \tag{119}$$

Since spatial and temporal discretizations are consistent, we conclude that given a well-prepared initial data at time step n, our numerical scheme is asymptotic preserving.

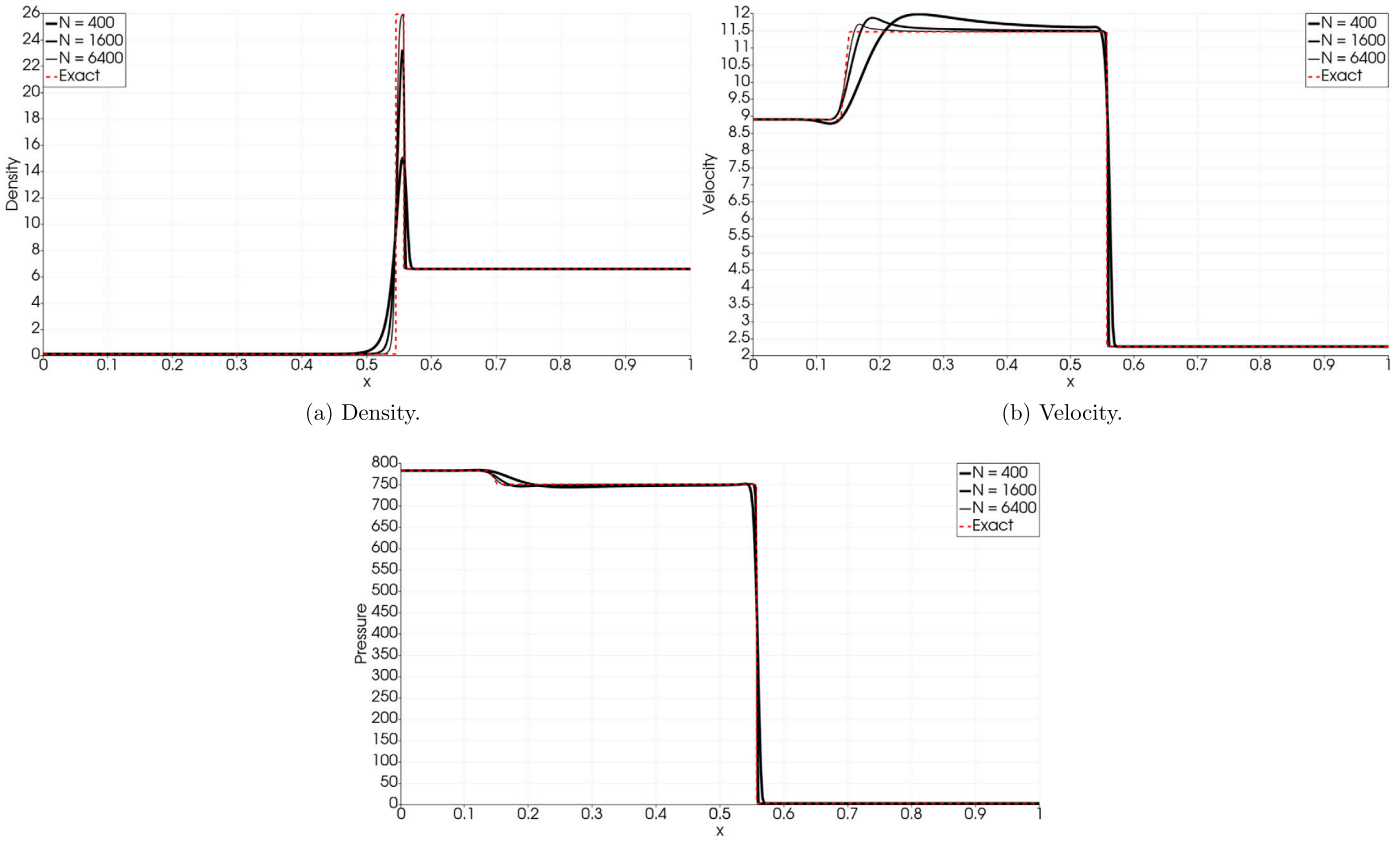

(a) Density.

(b) Velocity.

(c) Pressure.

Fig. 1. Peak test case. Results at time $T = 0.0039$ computed with different grid resolutions. (For interpretation of the colors in the figure(s), the reader is referred to the web version of this article.)

6. Numerical experiments

In this section we present a collection of numerical experiments in both one and two-dimensions. In order to demonstrate the capabilities of our all-Mach scheme, numerical experiments are conducted both in the highly compressible regime and in the incompressible (low-Mach) limit.

Unless otherwise stated, all simulations are performed using a second order scheme with HLL numerical fluxes, piecewise linear reconstruction of primitive variables, minmod slope limiter and the Courant number is $C = 0.8$.

6.1. Single phase flow

We start presenting some numerical results for single phase flows. In our numerical scheme, single phase flows can be simulated by using the same fluid properties, by assigning the same initial condition to all phases and setting volumetric fraction to a constant value in whole computational domain. In such cases, it is trivial to show that each phase and mixture quantities obey the standard compressible Euler equations. Since our numerical method is consistent with model equations, this behavior is maintained also at the discrete level, and our numerical scheme becomes *de-facto* an all-Mach solver for single-phase compressible flows.

6.1.1. Peak

The first test in the highly compressible regime consists of a Riemann problem whose solution is characterized by a narrow density peak which is hard to capture accurately. The initial condition is given by:

$$\rho_L = 0.1261192, \qquad u_L = 8.9047029, \qquad p_L = 782.92899,$$

$$\rho_R = 6.591493, \qquad u_R = 2.2654207, \qquad p_R = 3.1544874,$$

and the initial discontinuity is located at $x_0 = 0.5$.

In Fig. 1 the numerical solutions at time $T = 0.0039$ are compared with the exact solution. Numerical solution is computed using a first order scheme (Rusanov fluxes) and free-flow boundary conditions. In Table 1, we report the order of convergence of our method for density, momentum and pressure computed on computational grids of different sizes (from 400 to 6400 computational cells). The error (e) between the numerical and exact solutions is computed in L_1 norm. The (asymptotic) order of convergence is estimated as: $\theta_i = \log(e_i/e_{i+1})/\log(\Delta x_i/\Delta x_{i+1})$ and is reported in Table 1.

Table 1
Errors computed in L_1 norm and estimates of spatial convergence rate.

N	ρ		p		ρu	
	error	order	error	order	error	order
400	0.313	—	4.962	—	3.778	—
800	0.241	0.373	2.976	0.737	2.874	0.394
1600	0.174	0.468	1.703	0.805	2.058	0.482
3200	0.122	0.513	0.962	0.823	1.434	0.520
6400	0.084	0.540	0.515	0.901	0.982	0.546

6.1.2. Colella blast wave

The second test case in the highly compressible regime is the Woodward-Colella blast wave ([31] and [38]). Due to the strong interaction between shocks and rarefaction waves, this test case represents a golden standard to assess the robustness of a numerical scheme. This problem is characterized by the interaction between shock/rarefaction

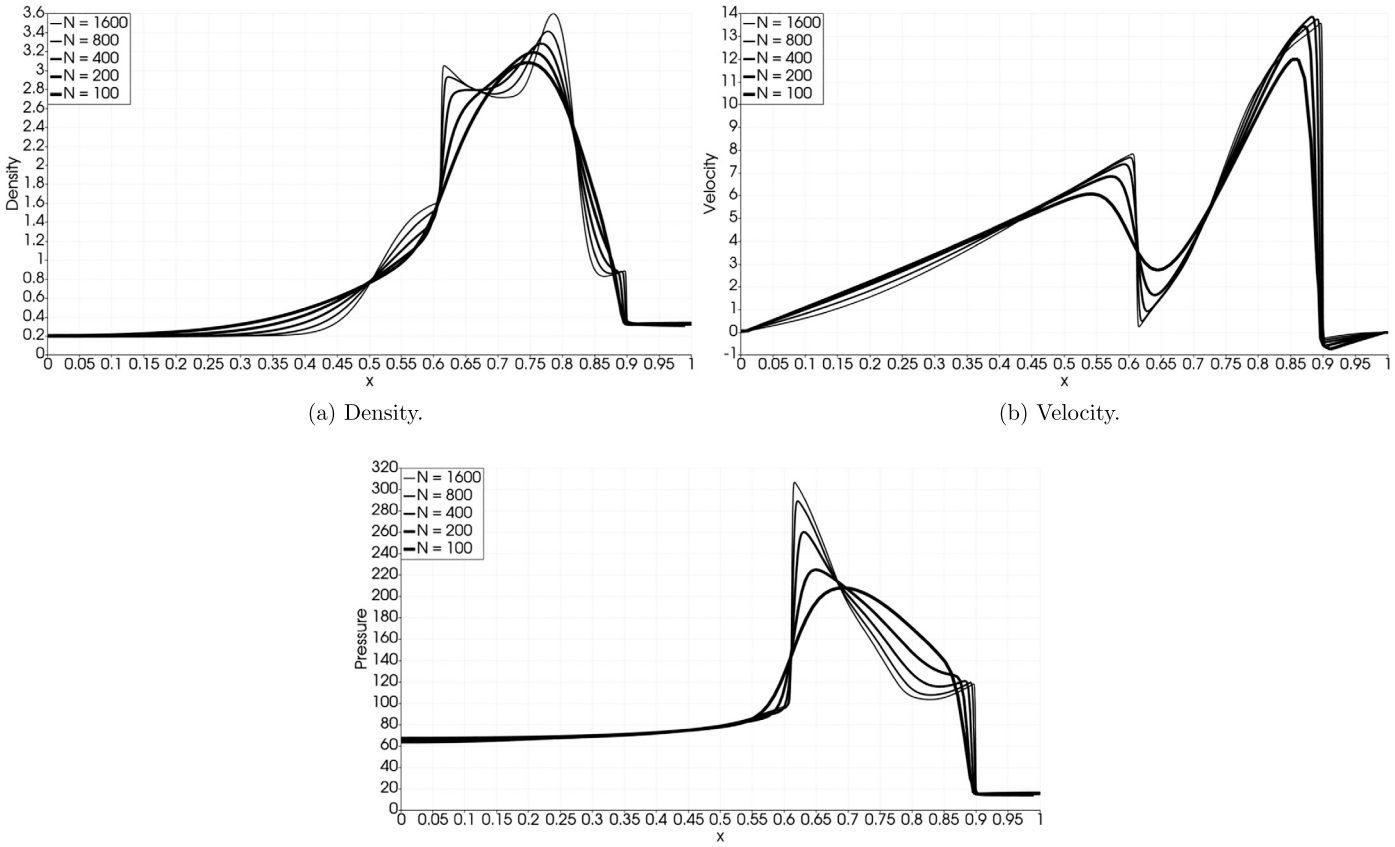

(a) Density. (b) Velocity.

(c) Pressure.

Fig. 2. Colella Blast Wave test case. Results at time $T = 0.038$ for different grid resolutions.

waves resulting from two Riemann problems solved in the interval $x \in [0, 1]$. The initial conditions are:

$$\begin{aligned}
&\rho_L = 1.0, \quad && u_L = 0.0, \quad && p_L = 1000., \quad && \text{if } 0.0 \le x \le 0.1 \\
&\rho_C = 1.0, \quad && u_C = 0.0, \quad && p_C = 0.01, \quad && \text{if } 0.1 < x \le 0.9 \\
&\rho_R = 1.0, \quad && u_R = 0.0, \quad && p_R = 100. \quad && \text{if } 0.9 < x \le 1.0
\end{aligned}$$

For this test case we use a first order scheme (Rusanov fluxes) and reflective boundary conditions. Fig. 2 shows the numerical solution at final integration time $T = 0.038$ computed on several computational grids with a resolution ranging from 100 to 1600 computational cells.

As shown in Fig. 2, our numerical scheme is able to robustly simulate all the (non-linear) interactions between waves and wall reflections. From a qualitatively point of view our numerical solution agrees very well with benchmark results reported in [38] as the computational grid is refined.

6.1.3. Gresho vortex

To demonstrate the accuracy of our method in the incompressible limit, we now present a numerical experiment in the low-Mach regime. We compute the numerical solution of the Gresho vortex ([39], [40] and [41]), a known stationary solution of the compressible Euler equations. This test case consists of a rotating vortex where centripetal forces are balanced exactly by pressure gradients. The vortex is centered at $(0.5, 0.5)$ and the computational domain is $[0, 1]^2$. The steady solution is given by:

$$\mathbf{u} = \mathbf{e}_\theta \begin{cases} 5r, & r \le 0.2 \\ 2 - 5r, & 0.2 < r < 0.4 \\ 0, & \text{otherwise} \end{cases} \tag{120}$$

$$p = \begin{cases} p_c + 25r^2/2, & r \le 0.2 \\ p_c + 4\ln(5r) + 4 - 20r + \frac{25r^2}{2}, & 0.2 < r < 0.4 \\ p_c + 4\ln(2) - 2, & \text{otherwise} \end{cases} \tag{121}$$

The density is uniform $\rho = 1$, $p_c = \frac{1}{\gamma M^2} - \frac{1}{2}$, $\gamma = 5/3$ and $r = \sqrt{x^2 + y^2}$ is the radial coordinate. The flow regime (low vs. high compressible) can be controlled by adjusting the numerical value of the Mach number, M. Numerical solution is computed using periodic boundary conditions and a computational grid of 80×80 cells. Fig. 3a shows the numerical solution obtained for $M = 0.01$ at the final integration time, $T = 3$ compared to the initial condition. Fig. 3b shows the vortex profile along the horizontal center-line of the computational domain at different final times.

As can be observed in Fig. 3, despite a small amount of numerical dissipation, the second order numerical scheme is capable of maintaining the vortex profile almost intact, even for long integration times. To further check the quality of the solution, we monitor the loss of kinetic energy. In Fig. 4 we show the ratio between the initial kinetic energy $E_{kin,0}$ and the kinetic energy at different times $E_{kin,t}$. The ratio between the initial and the final value is 0.8576 meaning that around 14% of the kinetic energy is dissipated due to the numerical integration. In Table 2, we report an estimate of the convergence order of our scheme. The error is computed by comparing the numerical solution at time $T = 1$ with the exact solution (120) and (121).

6.2. Two-phase flow

In this section, we present some numerical experiment for two-phase flows both in the compressible and incompressible regime.

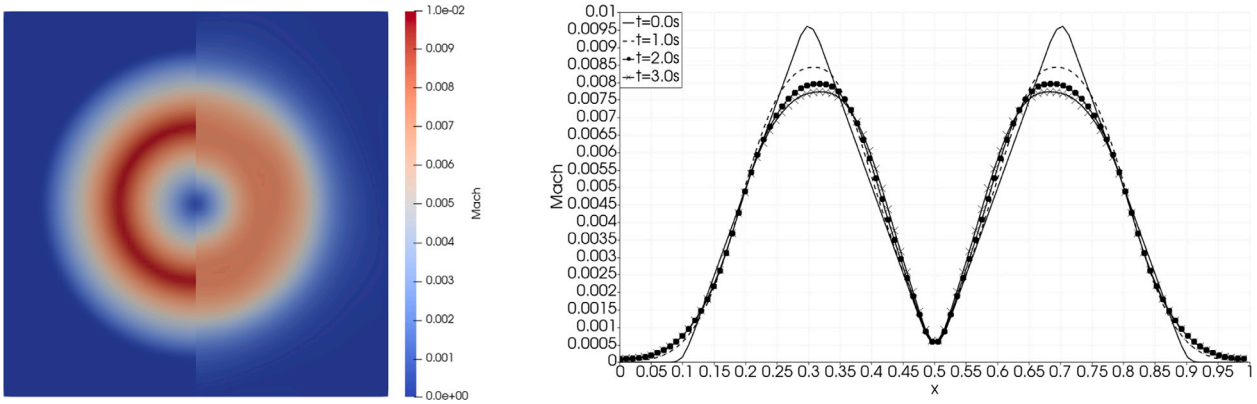

(a) Initial (left) and final (right) profile of the Mach number.

(b) Temporal evolution of the Mach number at the horizontal center-line of the domain.

Fig. 3. Temporal evolution of the Gresho vortex.

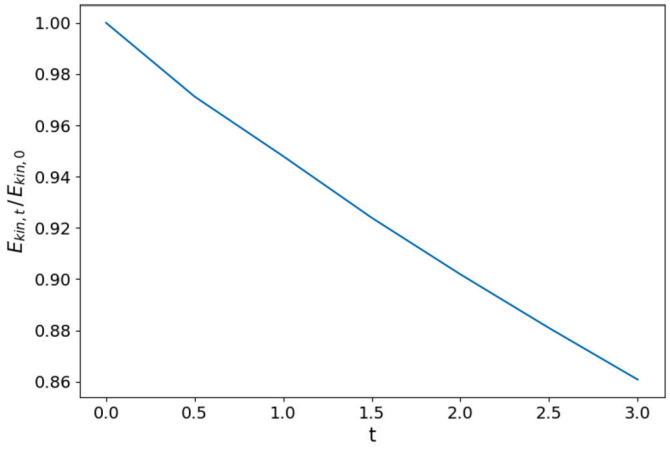

Fig. 4. Time evolution of the loss of kinetic energy.

Table 2
Errors computed in L_1 norm and estimates of the spatial convergence rate.

N	*Mach*		*p*		*E*	
	error	order	error	order	error	order
20×20	0.001	—	1.080e-1	—	1.736e-1	—
40×40	4.790e-4	1.196	1.641e-2	2.719	2.968e-2	2.548
80×80	2.317e-4	1.047	5.308e-3	1.628	9.140e-3	1.699
160×160	1.078e-4	1.102	1.675e-3	1.663	3.750e-3	1.285
320×320	4.072e-5	1.405	4.375e-4	1.937	8.593e-4	2.125

6.2.1. Water air shock tube

The first test case is taken from [23] and consists of a tube filled with highly pressurized liquid water (left-hand side of the computational domain) and air (right-hand side). Due to the strong pressure imbalance between phases, numerical methods which do not account for pressure relaxation fail after few time steps. In this scenario, when phasic pressures are estimated with poor accuracy, spurious oscillations appear in the numerical solution which may lead to negative values for pressure and therefore cause numerical instabilities. For these reasons, the water-air shock tube problem represents a good benchmark to assess both accuracy and robustness of our numeric scheme.

Each phase is governed by the equation of state for stiffened gas. The initial data and constants for liquid water (subscript l) and air (subscript g) are:

$$\rho_l = 1000\,\text{kg/m}^3, \quad p_l = 10^9\,\text{Pa}, \quad u_l = 0\,\text{m/s}, \quad \beta_l = 3.4,$$
$$\eta_l = 2.64\cdot10^9\,\text{Pa}, \quad \rho_g = 1\,\text{kg/m}^3, \quad p_g = 10^5\,\text{Pa},$$
$$u_g = 0\,\text{m/s}, \quad \beta_g = 0.4, \quad \eta_g = 0\,\text{Pa}$$

Volumetric fractions at the initial time are given by:

$$\alpha_l = \begin{cases} 1-\varepsilon, & \text{if } x < 0.7 \\ \varepsilon & \text{otherwise} \end{cases}$$

where $\varepsilon = 10^{-8}$ and $\alpha_g = 1-\alpha_l$.

Note that, in addition to the strong pressure and density difference between phases, right and left states at initial time contain almost pure phases. This represents the equivalent of *near-vacuum* states in the standard compressible Euler equations. For this test case, we use free-flow boundary conditions and instantaneous velocity and pressure relaxations. Fig. 5 shows the numerical solution at time $T = 229\,\mu$s computed on a computational grid of 1600 cells.

Our numerical solution is characterized by a significant numerical dissipation at the material interface (Fig. 5a). This is due to the fact that in the highly compressible regime our numerical scheme is equivalent to a standard explicit finite volume method, where the time step is controlled by the speed of fastest waves (typically associated to the least compressible phase). Consequently, waves traveling at a much smaller speed (e.g. contact discontinuities) are affected by significant numerical dissipation. Nonetheless, results obtained with our numerical scheme are consistent with those in [23].

6.2.2. Sedimentation

This test case represents a simplified setup for the separation process of a heavy and a light phase (subscript l and g, respectively) under the effect of gravity (see [42] and [43]). The goal of this test case is to assess the capabilities of our numerical scheme to resolve countercurrent flows in regions characterized by small volumetric fractions and low Mach number.

The domain is one-dimensional and represents a closed vertical tube 7.5 m long. The tube is initially filled with a stagnant mixture of heavy and light fluids in equal quantities, that is:

$$u_l = u_g = 0\,\text{m/s}$$
$$\alpha_l = \alpha_g = 0.5$$
$$p_l = p_g = 10^5\,\text{Pa}.$$

The equation of state for perfect gases is used for both phases. The ratio of specific heats is $\gamma_g = 1.4$ and $\gamma_l = 4.4$, respectively. Reflective boundary conditions are used to simulate closed wall. The gravity

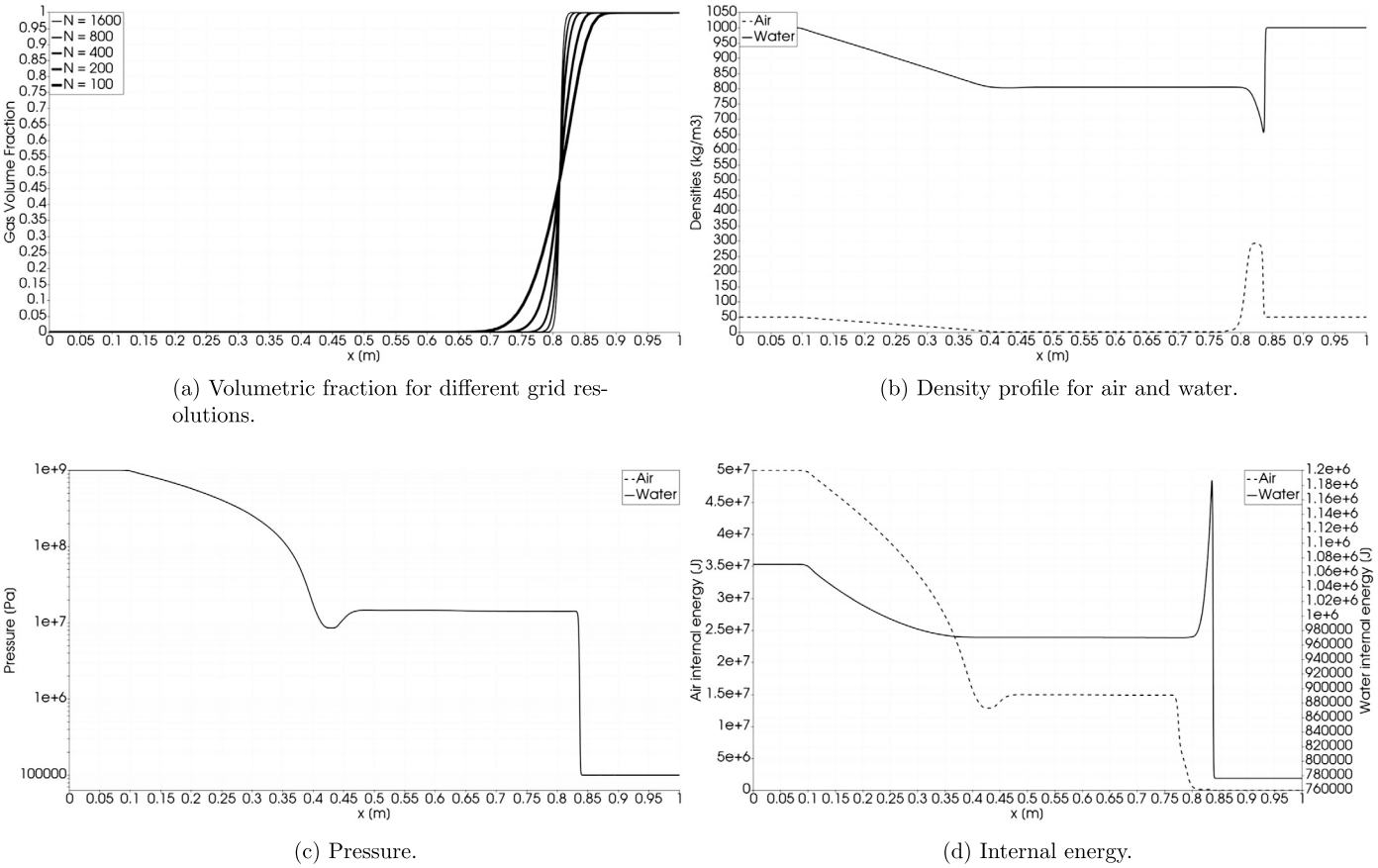

(a) Volumetric fraction for different grid resolutions.

(b) Density profile for air and water.

(c) Pressure.

(d) Internal energy.

Fig. 5. Water-air shock tube. Numerical solution at $T = 229\,\mu s$.

constant is set to $g = 9.81\,m/s^2$. Finally, densities for both phases are $\rho_l = 3\,kg/m^3$ and $\rho_g = 1\,kg/m^3$.

For this test case, we are interested in the final steady state, where the heavy phase is precipitated in the bottom half of the domain, while the light phase occupies the upper half of the tube. The corresponding profile of volumetric fractions is characterized by a (steady) discontinuity approximately located in the middle of the computational domain.

For this test case, we employ a instantaneous pressure relaxation model. However, both phases are allowed to have different velocities. Numerical results are obtained using a computational grid of 100 cells and a fixed ratio $\Delta t/\Delta x = 6.0e-4$ as done in [42].

Fig. 6a shows the time evolution of volumetric fraction for the gaseous phase. Again, in our numerical results, the contact discontinuity between phases is smeared out due to the presence of additional numerical dissipation in the volumetric fraction equation. Nonetheless, at the final integration time, $T = 1.5\,s$, the numerical solution approaches the expected steady state. Due to small compressibility effects, the interface between phases is not exactly located in the middle of the computational domain. This effect is observed also by [43]. Lastly, in Fig. 6b we report the time evolution of the pressure profile at different time steps.

6.2.3. Water faucet

In this test case, the computational domain is represented by a 12 m long vertical tube filled with water and air. The initial conditions for the liquid and gas are:

$$u_l = 10\,m/s \qquad \rho_l = 1000\,kg/m^3 \qquad \alpha_l = 0.8 \qquad p_l = 10^5\,Pa$$
$$u_g = 0\,m/s \qquad \rho_g = 1\,kg/m^3 \qquad \alpha_g = 0.2 \qquad p_g = 10^5\,Pa$$

The equation of state for perfect gases is used for water vapor with $\gamma_g = 1.4$. The equation of state for stiffened gases is used for water. Numerical parameters are the same as those used in the water-air shock tube problem. As in the previous test case, both phases are in the incompressible limit.

Due to the effect of gravity, a triangular wave develops in the water jet. As noted in [23], the Baer-Nunziato model is overly complicated for this problem, and other (more effective) solvers can be found in literature (see for instance [44]). Nonetheless, this test case is selected to demonstrate the capabilities of our numerical scheme to simulate two-phase flows also in the low-Mach regime.

To simulate the time evolution of the water faucet, instantaneous pressure relaxation is used, however both phases are not constrained to have the same velocity (as done in [23] and [42]).

Fixed water velocity $u_l = 10\,m/s$, water volumetric fraction $\alpha_l = 0.8$ and vapor velocity $u_g = 0\,m/s$ are imposed at the top of the tube. At the lower boundary, a pressure outlet boundary condition is used ($p = 10^5$ Pa). The gravity constant is set to $g = 9.81\,m/s^2$.

To facilitate comparisons with numerical results reported in [42], in Fig. 7a, we show the volumetric fraction of vapor at time $t = 0.4\,s$ for both first and second order numerical schemes (HLL numerical fluxes, $\Delta t/\Delta x = 5.0e-4$ and 100 computational cells).

This problem has an analytical solution if pressure variations in the vapor are ignored (see [45]). The analytic expression for the volumetric fraction of vapor is given by:

$$\alpha_g^e(x,t) = \begin{cases} 1 - \dfrac{\alpha_l^e u_l^e}{\sqrt{2gx + (u_l^e)^2}}, & \text{if } x \le u_l^e t + \dfrac{gt^2}{2} \\ 0.2, & \text{otherwise,} \end{cases} \tag{122}$$

where $u_l^e = 10\,m/s$ and $\alpha_l^e = 0.8$. Lastly, the time evolution of liquid velocity along the tube at various time step is shown in Fig. 7b.

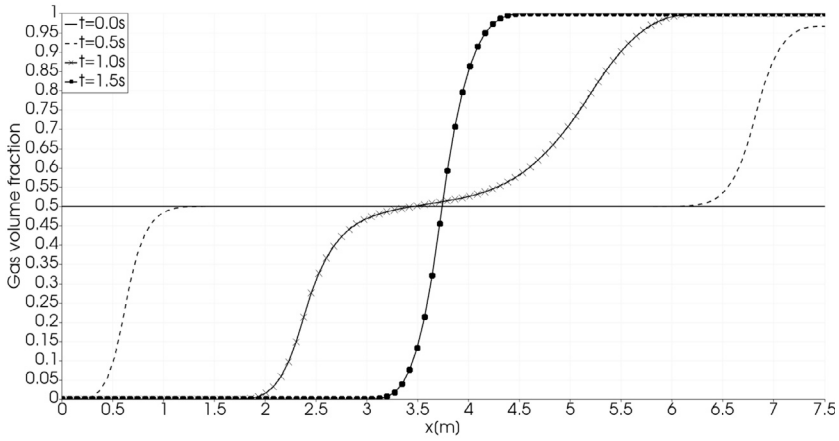

(a) Volumetric fraction.

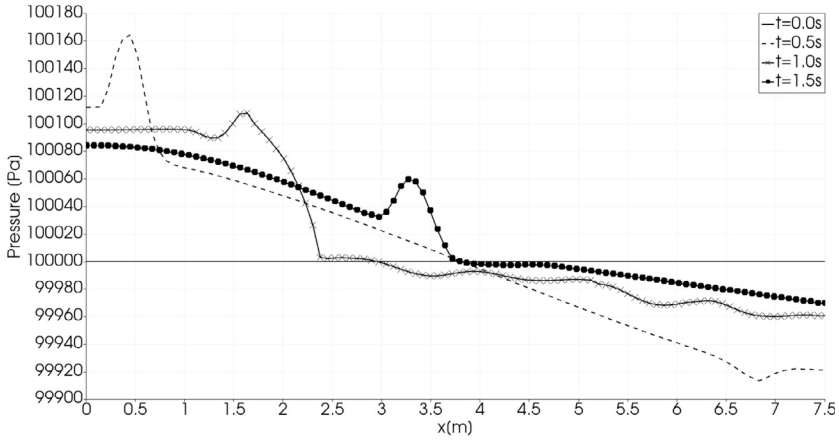

(b) Pressure.

Fig. 6. Sedimentation test. Volumetric fraction and pressure profiles at different time steps.

Once again, our numerical results are in agreement with those presented in [42] and [23], and our numerical scheme is capable of simulating correctly the transient dynamics also in the incompressible limit.

6.2.4. Rayleigh-Taylor instability

The Rayleigh-Taylor instability is encountered in a broad range of industrial and natural processes, such as plasma fusion reactors and ocean dynamics. The instability takes place at the interface between two fluids with different densities, and arises when a small perturbation appears at the material interface which separates a heavy fluid (located in the top half region of the domain) from a light fluid (bottom half of the computational domain). Due to the effect of gravity, the heavy fluid (subscript l) insinuates in the region occupied by the light fluid (subscript g) and pushes the lighter fluid in top half of the domain. During this process, the material interface is stretched and deformed while the system seeks to reduce the potential energy. Furthermore, due to the difference in the shear velocity between phases across the material interface, secondary instabilities develop, such as the Kelvin-Helmholtz instability.

In this test case, the rectangular domain is a $[0,1\,\mathrm{m}]\times[0,2\,\mathrm{m}]$ and reflective boundary conditions are used to model solid walls. The initial data is given by:

$$\rho_g = 1\,\mathrm{kg/m^3}, \qquad u_g = 0\,\mathrm{m/s}, \qquad p_g = 10^5\,\mathrm{Pa},$$
$$\rho_l = 5\,\mathrm{kg/m^3}, \qquad u_l = 0\,\mathrm{m/s}, \qquad p_l = 10^5\,\mathrm{Pa}.$$

The initial profile of the material interface is given by:

$$y(x) = y_c + \frac{0.02}{\sigma\sqrt{2\pi}} e^{-\frac{x-\mu}{2\sigma^2}}$$

where $y_c = 1$, $\sigma = 0.08$ and $\mu = 0.5$.

In the lower part of the domain $\alpha_g = 1-\varepsilon$, while in the upper part $\alpha_g = \varepsilon$ and $\varepsilon = 10^{-4}$. The equation of state for perfect gasses is used for the light fluid, while the stiffened EOS with $\eta_l = 5\cdot 10^5$ Pa is used for the heavy phase. The gravity constant is set to $g = 90\,\mathrm{m/s^2}$ to produce an accelerated dynamic of the material interface.

To simulate the dynamic of this instability, instantaneous pressure and velocity relaxations are used. The computational grid consists of 300×600 cells. In Fig. 8, we see the development of the primary instability as well as some secondary Kelvin-Helmholtz instabilities appearing in later time steps due to the difference in the shear velocity between the two phases.

6.2.5. Bubble drop

This test can be found in [8] and describes the dynamic of a heavy bubble (subscript l) dropping inside a lighter fluid (subscript g) under the effect of gravity ($g = 90\,\mathrm{m/s^2}$ for this case). This test case represents a benchmark to assess the capability of a numerical scheme to simulate two-phase flows characterized by very low Mach numbers, while preserving at the same time a moving contact discontinuity.

For this test case the computational domain is a closed box of dimensions $[0,1\,\mathrm{m}]\times[0,2\,\mathrm{m}]$. The bubble is initially located at $(0.5\,\mathrm{m}, 1.7\,\mathrm{m})$

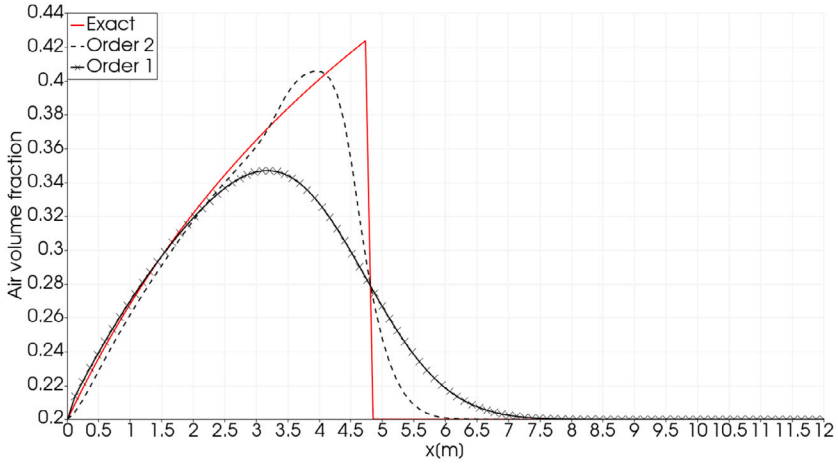

(a) Air volume fraction at t=0.4s for first (solid line) and second order (dashed line) schemes. Exact solution is shown in red.

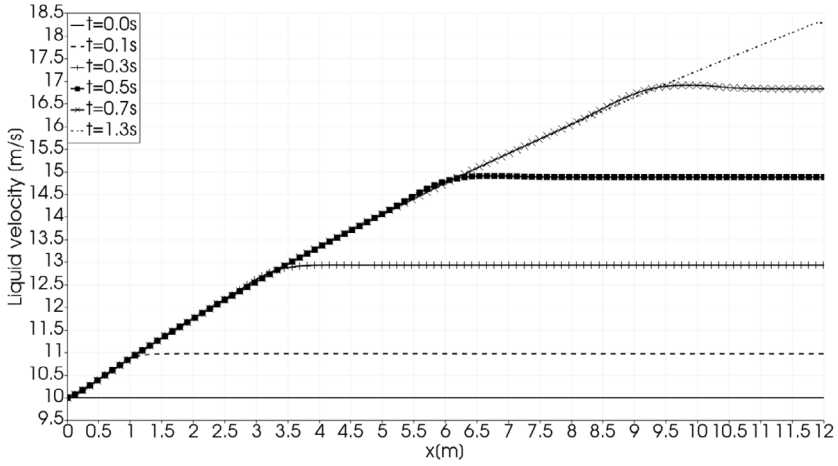

(b) Liquid velocity at different time steps.

Fig. 7. Water faucet test case.

and has a radius of 0.2 m. Reflective boundary conditions are imposed at solid walls. The initial conditions are:

$$\rho_g = 1\,\text{kg/m}^3, \qquad u_g = 0\,\text{m/s}, \qquad p_g = 10^5\,\text{Pa}$$

$$\rho_l = 4\,\text{kg/m}^3, \qquad u_l = 0\,\text{m/s}, \qquad p_l = 10^5\,\text{Pa}$$

everywhere. Volume fractions are $\alpha_l = 1-\varepsilon$ inside the bubble and $\alpha_l = \varepsilon$ outside, with $\varepsilon = 10^{-4}$. Perfect gas EOS is used for both fluids with $\gamma_g = 1.4$ and $\gamma_l = 4.4$. In Fig. 9 the time evolution of the bubble is shown on a computational grid of 50×100 cells as done in [8]. Note that in the long run, numerical dissipation affects the solution and blurs the bubble profile. This happens to a lower extent also in [8]. Nonetheless, the interface instabilities are still visible at the final integration time. In Fig. 10, the same test case is reproduced on a finer grid of 200×400 cells and shows a sharper resolution of the contact interface.

6.2.6. Dam break

The dam break test is another problem involving unsteady flows in the weakly compressible regime (see [10], [8], [46]). The initial configuration consists of a water column (subscript l) located in the region $[0, 0.06\,\text{m}] \times [0, 0.12\,\text{m}]$. Water is surrounded by air (subscript g). The computational domain is a closed box of dimensions $[0, 0.5\,\text{m}] \times [0, 0.15\,\text{m}]$ and the initial condition is:

$$\rho_g = 1\,\text{kg/m}^3, \qquad u_g = 0\,\text{m/s}, \qquad p_g = 10^5\,\text{Pa}$$

$$\rho_l = 1000\,\text{kg/m}^3, \qquad u_l = 0\,\text{m/s}, \qquad p_l = 10^5\,\text{Pa}.$$

Volumetric fractions at the initial time are $\alpha_l = 1-\varepsilon$ inside the column and $\alpha_l = \varepsilon$ in the rest of the domain, with $\varepsilon = 10^{-3}$. The equation of state for perfect gases is used for air with $\gamma_g = 1.4$. The equation of state for stiffened gases is used for water. Numerical parameters are the same as those used in the water-air shock tube problem. As in the previous test case, both phases are in the incompressible limit. Under the effect of gravity ($g = 9.81\,\text{m/s}^2$), the heavy column collapses and moves to the right region of the domain producing a sloshing dynamics. The computational domain is discretized with 200×60 cells, and reflective boundary conditions are applied at domain boundaries.

Fig. 11 shows the volumetric fraction of the liquid phase at times $t = 0\,\text{s}, 0.066\,\text{s}, 0.109\,\text{s}, 0.164\,\text{s}, 0.222\,\text{s}, 0.281\,\text{s}$. Again the contact discontinuity is smeared out due to the effect of numerical dissipation, however the sloshing dynamics is still visible.

6.2.7. Bubble ascension

This test case is found in [10] and [8]. It describes the ascension of a light air bubble (subscript g) inside a closed box filled with water (subscript l) under the effect of gravity ($g = 9.81\,\text{m/s}^2$). This test case presents several numerical difficulties. It is characterized by very low Mach numbers (equal to zero at time $t = 0\,\text{s}$ and increasing up to 10^{-1}

(a) time step=0 (b) time step=2000 (c) time step=4000

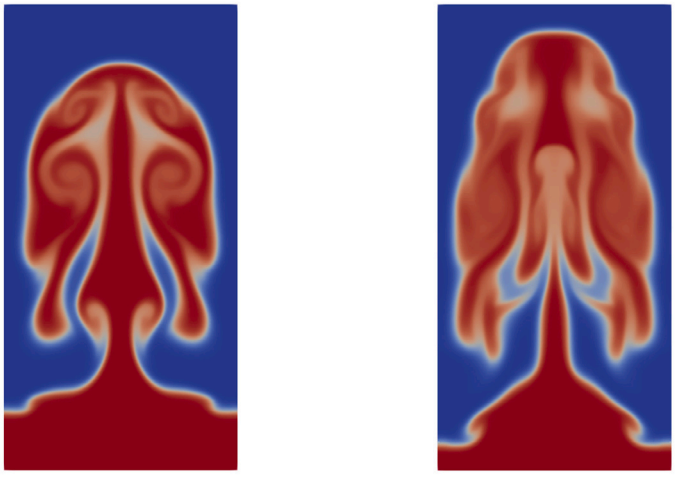

(d) time step=6000 (e) time step=8000

Fig. 8. Rayleigh-Taylor instability, volume fractions at different time steps.

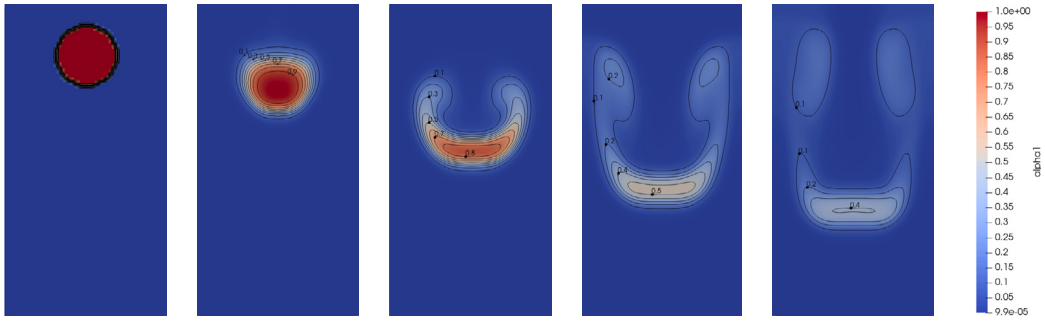

(a) t=0.0s (b) t=0.1s (c) t=0.2s (d) t=0.3s (e) t=0.4s

Fig. 9. Dropping bubble. Time evolution of volumetric fraction (coarse grid).

during the simulation) and a density ration between the two fluids equal to 1000 ($\rho_g = 1\,\text{kg/m}^3$ and $\rho_l = 1000\,\text{kg/m}^3$).

For this test case the computational domain has dimensions $[0, 2\,\text{m}] \times [0, 2\,\text{m}]$. The bubble is initially located at $(1.0\,\text{m}, 0.3\,\text{m})$ and has a radius of 0.2 m. Reflective boundary conditions are imposed at solid walls. At the beginning of the simulation fluids are at rest and the pressure field has an hydrostatic profile. Volume fractions are $\alpha_g = 1 - \varepsilon$ inside the bubble and $\alpha_g = \varepsilon$ outside, with $\varepsilon = 10^{-3}$. Perfect gas EOS is used for air with $\gamma_g = 1.4$. Stiffened gas EOS is used for water with the same parameters as those used in the water-air shock tube problem. In Fig. 12 the time evolution of the bubble is shown on a computational grid of 400×400 cells. As for the other tests, in the long run, numerical dissipation affects the solution and blurs the bubble profile. Nonetheless, the interface instabilities are still visible at the final integration time.

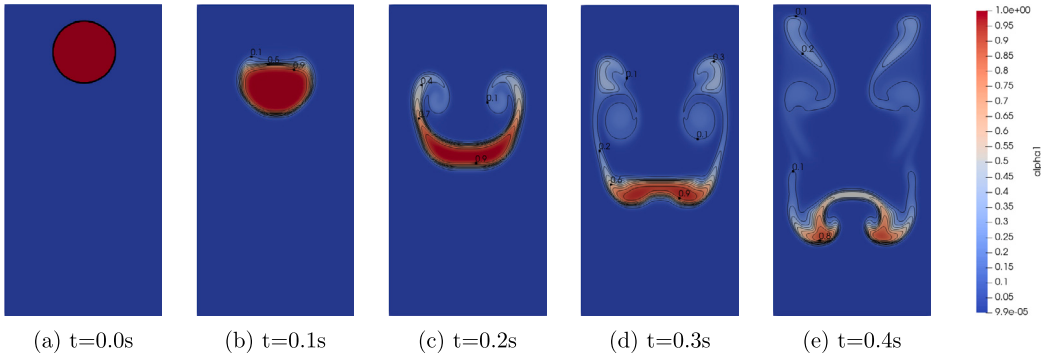

Fig. 10. Dropping bubble. Time evolution of volumetric fraction (fine grid).

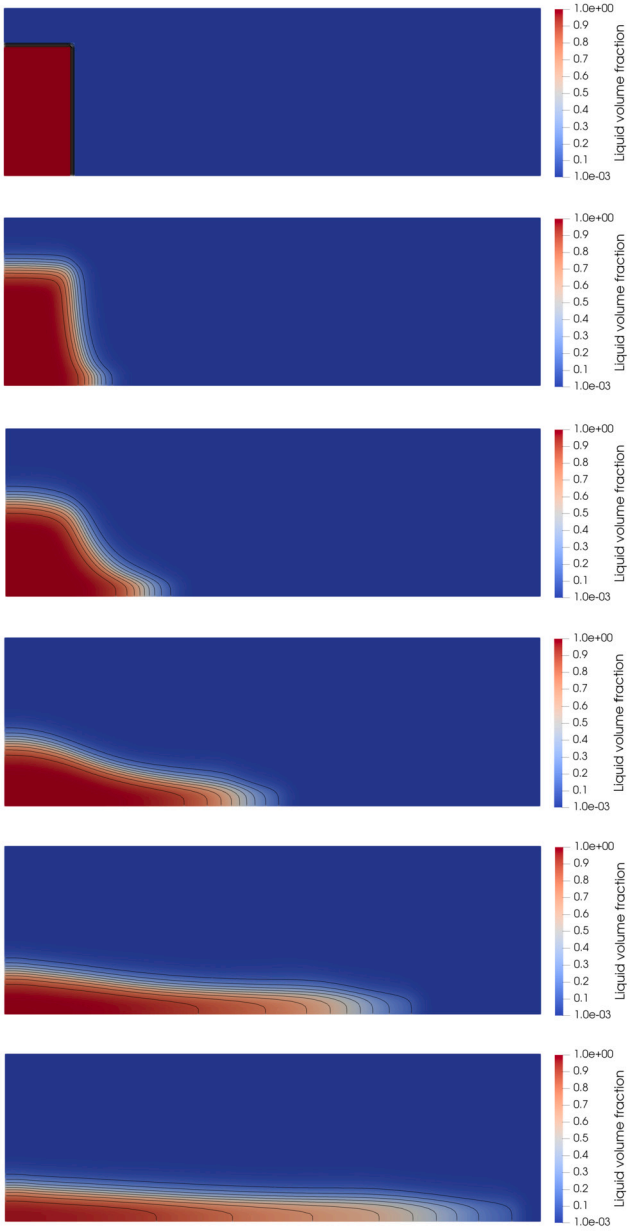

Fig. 11. Dam break. Time evolution of volumetric fraction of the liquid phase.

7. Conclusions

In this work, we propose a well-balanced Implicit-Explicit Runge-Kutta numerical scheme for the efficient simulation of the Baer-Nunziato model at all-Mach regimes. The numerical method is based on the explicit treatment of non-stiff terms, while stiff terms are kept implicit to remove the time step restriction stemming from acoustic waves. By introducing suitable linearizations in the semi-discrete energy equation obtained in the framework of a IMEX-RK time discretization, a predictor-corrector scheme was derived where the implicit contribution of pressure waves is accounted for by solving a system of non-linear elliptic equations in the unknown phasic pressures. A well-balanced discretization of non-conservative terms was also introduced, resulting in a numerical scheme capable of preserving steady-state solutions, including the so-called "lake-at-rest" state. Finally, we proved that our numerical scheme is asymptotic-preserving. Compared to standard explicit finite volume schemes, the time step of our method is driven by the mean flow velocity and not by the speed of acoustic waves. Moreover, the proposed approach is characterized by a lower computational complexity if compared to fully (monolithic) implicit schemes, since the implicit correction only requires to solve a system of non-linear elliptic equations. Numerical results demonstrate the capabilities of our numerical scheme to correctly capture shocks in the high Mach regime as well as to efficiently simulate flows at low Mach numbers.

In future work, the scheme will be generalized to cope with more general and non-linear EOS. We aim at extending the scheme by including other approximate Riemann solvers to achieve sharper resolution of contact discontinuities and material interfaces.

CRediT authorship contribution statement

Sandro Malusà: Data curation, Formal analysis, Software, Visualization, Writing – original draft, Conceptualization, Methodology. **Alessandro Alaia:** Funding acquisition, Project administration, Supervision, Writing – review & editing, Conceptualization, Methodology.

Declaration of competing interest

The authors declare that they have no known competing financial interests or personal relationships that could have appeared to influence the work reported in this paper.

Data availability

No data was used for the research described in the article.

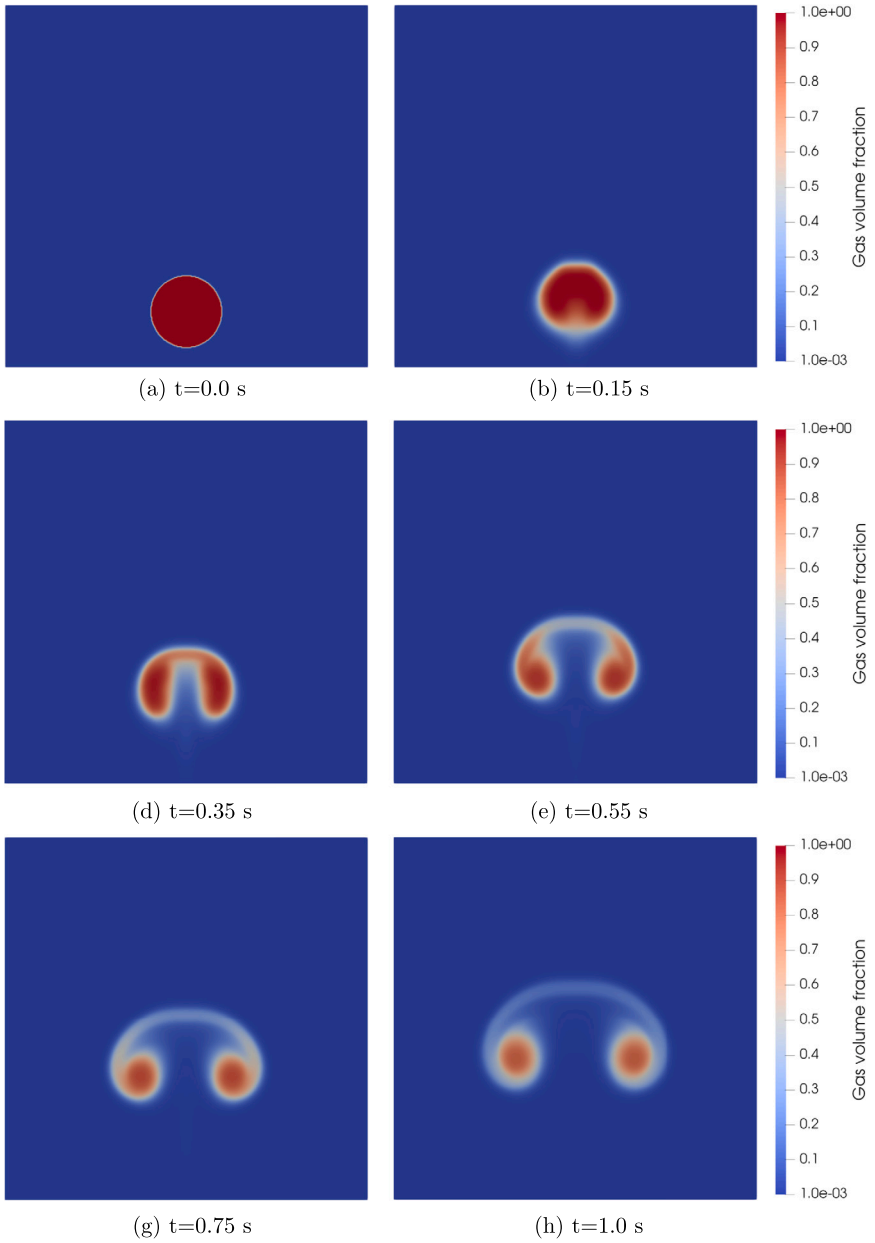

Fig. 12. Bubble ascension. Time evolution of volumetric fraction of the gasnon phase.

Acknowledgements

The authors wish to thank Gabriella Puppo for fruitful discussions and valuable feedback.

References

[1] M. Thema, T. Weidlich, M. Hörl, A. Bellack, F. Mörs, F. Hackl, M. Kohlmayer, J. Gleich, C. Stabenau, T. Trabold, M. Neubert, F. Ortloff, R. Brotsack, D. Schmack, H. Huber, D. Hafenbradl, J. Karl, M. Sterner, Biological CO2-methanation: an approach to standardization, Energies 12 (9) (2019), https://doi.org/10.3390/en12091670, https://www.mdpi.com/1996-1073/12/9/1670.

[2] M. Baer, J. Nunziato, A two-phase mixture theory for the deflagration-to-detonation transition (ddt) in reactive granular materials, Int. J. Multiph. Flow 12 (6) (1986) 861–889, https://doi.org/10.1016/0301-9322(86)90033-9, https://www.sciencedirect.com/science/article/pii/0301932286900339.

[3] D. Drew, S. Passman, Theory of Multicomponent Fluids, Applied Mathematical Sciences, Springer New York, 2006, https://books.google.it/books?id=sccFCAAAQBAJ.

[4] Richard Saurel, F. Petitpas, R.A. Berry, Simple and efficient relaxation methods for interfaces separating compressible fluids, cavitating flows and shocks in multiphase mixtures, J. Comput. Phys. 228 (5) (2009) 1678–1712, https://doi.org/10.1016/j.jcp.2008.11.002, https://www.sciencedirect.com/science/article/pii/S0021999108005895.

[5] M. Pelanti, K.-M. Shyue, A mixture-energy-consistent six-equation two-phase numerical model for fluids with interfaces, cavitation and evaporation waves, J. Comput. Phys. 259 (2014) 331–357, https://doi.org/10.1016/j.jcp.2013.12.003, https://www.sciencedirect.com/science/article/pii/S0021999113008024.

[6] M. Pelanti, Low Mach number preconditioning techniques for Roe-type and hllc-type methods for a two-phase compressible flow model, Appl. Math. Comput. 310 (2017) 112–133, https://doi.org/10.1016/j.amc.2017.04.014, https://www.sciencedirect.com/science/article/pii/S0096300317302588.

[7] A. Kapila, R. Menikoff, J. Bdzil, S. Son, D. Stewart, Two-phase modeling of deflagration-to-detonation transition in granular materials: reduced equations, Phys. Fluids 13 (2001) 3002–3024, https://doi.org/10.1063/1.1398042.

[8] A. Murrone, H. Guillard, A five equation reduced model for compressible two phase flow problems, J. Comput. Phys. 202 (2) (2005) 664–698, https://doi.org/10.1016/j.jcp.2004.07.019, https://www.sciencedirect.com/science/article/pii/S0021999104003018.

[9] R. Saurel, F. Petitpas, R. Abgrall, Modelling phase transition in metastable liquids: application to cavitating and flashing flows, J. Fluid Mech. 607 (2008) 313–350, https://hal.inria.fr/inria-00333908.

[10] A. Murrone, H. Guillard, Behavior of upwind scheme in the low Mach number limit: III. Preconditioned dissipation for a five equation two phase model, Comput. Flu-

ids 37 (10) (2008) 1209–1224, https://doi.org/10.1016/j.compfluid.2006.12.010, https://www.sciencedirect.com/science/article/pii/S0045793008000054.
[11] B. Braconnier, B. Nkonga, An all-speed relaxation scheme for interface flows with surface tension, J. Comput. Phys. 228 (16) (2009) 5722–5739, https://doi.org/10.1016/j.jcp.2009.04.046, https://www.sciencedirect.com/science/article/pii/S0021999109002319.
[12] S. LeMartelot, B. Nkonga, R. Saurel, Liquid and liquid–gas flows at all speeds, J. Comput. Phys. 255 (2013) 53–82, https://doi.org/10.1016/j.jcp.2013.08.001, https://www.sciencedirect.com/science/article/pii/S0021999113005263.
[13] A.D. Demou, N. Scapin, M. Pelanti, L. Brandt, A pressure-based diffuse interface method for low-Mach multiphase flows with mass transfer, J. Comput. Phys. 448 (2022) 110730, https://doi.org/10.1016/j.jcp.2021.110730, https://www.sciencedirect.com/science/article/pii/S0021999121006252.
[14] V. Ransom, D. Hicks, Hyperbolic two-pressure models for two-phase flow, J. Comput. Phys. 53 (1) (1984) 124–151, https://doi.org/10.1016/0021-9991(84)90056-1, https://www.sciencedirect.com/science/article/pii/0021999184900561.
[15] W. Boscheri, G. Dimarco, M. Tavelli, An efficient second order all Mach finite volume solver for the compressible Navier-Stokes equations, Comput. Methods Appl. Mech. Eng. 374 (2021) 113602, https://doi.org/10.1016/j.cma.2020.113602, https://www.sciencedirect.com/science/article/pii/S0045782520307878.
[16] S. Avgerinos, F. Bernard, A. Iollo, G. Russo, Linearly implicit all Mach number shock capturing schemes for the Euler equations, J. Comput. Phys. 393 (2019) 278–312, https://doi.org/10.1016/j.jcp.2019.04.020, https://www.sciencedirect.com/science/article/pii/S0021999119302530.
[17] G. Bispen, M. Lukáčová-Medvidová, L. Yelash, Asymptotic preserving IMEX finite volume schemes for low Mach number Euler equations with gravitation, J. Comput. Phys. 335 (2017) 222–248, https://doi.org/10.1016/j.jcp.2017.01.020, https://www.sciencedirect.com/science/article/pii/S002199911730030X.
[18] E. Abbate, A. Iollo, G. Puppo, An asymptotic-preserving all-speed scheme for fluid dynamics and nonlinear elasticity, SIAM J. Sci. Comput. 41 (5) (2019) A2850–A2879, https://doi.org/10.1137/18M1232954, arXiv:https://doi.org/10.1137/18M1232954.
[19] J. Haack, S. Jin, J.G. Liu, An all-speed asymptotic-preserving method for the isentropic Euler and Navier-Stokes equations, Commun. Comput. Phys. 12 (10 2010), https://doi.org/10.4208/cicp.250910.131011a.
[20] M. Lukáčová-Medviďová, G. Puppo, A. Thomann, An all Mach number finite volume method for isentropic two-phase flow, arXiv:2202.01577, 02 2022.
[21] B. Re, R. Abgrall, A pressure-based method for weakly compressible two-phase flows under a Baer-Nunziato type model with generic equations of state and pressure and velocity disequilibrium, Int. J. Numer. Methods Fluids 94 (8) (2022) 1183–1232, https://doi.org/10.1002/fld.5087, arXiv:https://onlinelibrary.wiley.com/doi/pdf/10.1002/fld.5087, https://onlinelibrary.wiley.com/doi/abs/10.1002/fld.5087.
[22] L. Pareschi, G. Russo, Implicit-explicit Runge-Kutta schemes and applications to hyperbolic systems with relaxation, J. Sci. Comput. (2010), https://doi.org/10.48550/ARXIV.1009.2757, https://arxiv.org/abs/1009.2757.
[23] R. Saurel, R. Abgrall, A multiphase Godunov method for compressible multifluid and multiphase flows, J. Comput. Phys. 150 (2) (1999) 425–467, https://doi.org/10.1006/jcph.1999.6187, https://www.sciencedirect.com/science/article/pii/S0021999199961879.
[24] S. Jin, Efficient asymptotic-preserving (AP) schemes for some multiscale kinetic equations, SIAM J. Sci. Comput. 21 (2) (1999) 441–454, https://doi.org/10.1137/S1064827598334599, arXiv:https://doi.org/10.1137/S1064827598334599.
[25] S. Jin, Asymptotic preserving (AP) schemes for multiscale kinetic and hyperbolic equations: a review, Riv. Mat. Univ. Parma N.S. 2 (01 2010).
[26] H. Kai, J. Ari, K. Sirpa, K. Hannu, K. Markku, K. Antti, M. Mikko, T. Veikko, Multiphase flow dynamics, theory and numerics, VTT publications, no. 722, VTT Technical Research Centre of Finland, Finland, 2009.
[27] K. Lappalainen, Modelling gas-liquid flow in trickle-bed reactors, Doctoral thesis, Helsinki University of Technology, 2009, http://urn.fi/URN:ISBN:978-951-22-9886-0.
[28] G. Strang, On the construction and comparison of difference schemes, SIAM J. Numer. Anal. 5 (3) (1968) 506–517, https://doi.org/10.1137/0705041, arXiv:https://doi.org/10.1137/0705041.
[29] A. Harten, P.D. Lax, B. van Leer, On Upstream Differencing and Godunov-Type Schemes for Hyperbolic Conservation Laws, Springer Berlin Heidelberg, 1997, pp. 53–79.
[30] S.F. Davis, Simplified second-order Godunov-type methods, SIAM J. Sci. Stat. Comput. 9 (3) (1988) 445–473, https://doi.org/10.1137/0909030, arXiv:https://doi.org/10.1137/0909030.
[31] E. Toro, Riemann Solvers and Numerical Methods for Fluid Dynamics, Springer Berlin, Heidelberg, 1997.
[32] R. Saurel, R. Abgrall, A simple method for compressible multifluid flows, SIAM J. Sci. Comput. 21 (3) (1999) 1115–1145, https://doi.org/10.1137/S1064827597323749, arXiv:https://doi.org/10.1137/S1064827597323749.
[33] R. Abgrall, How to prevent pressure oscillations in multicomponent flow calculations: a quasi conservative approach, J. Comput. Phys. 125 (1) (1996) 150–160, https://doi.org/10.1006/jcph.1996.0085, https://www.sciencedirect.com/science/article/pii/S0021999196900856.
[34] J.M. Greenberg, A. Leroux, A well-balanced scheme for the numerical processing of source terms in hyperbolic equations, SIAM J. Numer. Anal. 33 (1) (1996) 1–16, https://doi.org/10.1137/0733001, arXiv:https://doi.org/10.1137/0733001.
[35] S. Noelle, N. Pankratz, G. Puppo, J.R. Natvig, Well-balanced finite volume schemes of arbitrary order of accuracy for shallow water flows, J. Comput. Phys. 213 (2) (2006) 474–499, https://doi.org/10.1016/j.jcp.2005.08.019, https://www.sciencedirect.com/science/article/pii/S002199910500389X.
[36] P. Helluy, J.M. Hérard, H. Mathis, A well-balanced approximate Riemann solver for compressible flows in variable cross-section ducts, J. Comput. Appl. Math. 236 (7) (2012) 1976–1992, https://doi.org/10.1016/j.cam.2011.11.008, https://www.sciencedirect.com/science/article/pii/S0377042711005784.
[37] C. Klingenberg, G. Puppo, M. Semplice, Arbitrary order finite volume well-balanced schemes for the Euler equations with gravity, SIAM J. Sci. Comput. 41 (2) (2019) A695–A721, https://doi.org/10.1137/18M1196704, arXiv:https://doi.org/10.1137/18M1196704.
[38] P. Woodward, P. Colella, The numerical simulation of two-dimensional fluid flow with strong shocks, J. Comput. Phys. 54 (1) (1984) 115–173, https://doi.org/10.1016/0021-9991(84)90142-6, https://www.sciencedirect.com/science/article/pii/0021999184901426.
[39] A. Thomann, G. Puppo, C. Klingenberg, An all speed second order well-balanced IMEX relaxation scheme for the Euler equations with gravity, J. Comput. Phys. 420 (2020) 109723, https://doi.org/10.1016/j.jcp.2020.109723, https://www.sciencedirect.com/science/article/pii/S0021999120304976.
[40] W. Barsukow, P. Edelmann, C. Klingenberg, F. Miczek, F. Roepke, A numerical scheme for the compressible low-Mach number regime of ideal fluid dynamics, J. Sci. Comput. 72 (08 2017), https://doi.org/10.1007/s10915-017-0372-4.
[41] R. Liska, B. Wendroff, Comparison of several difference schemes on 1D and 2D test problems for the Euler equations, SIAM J. Sci. Comput. 25 (3) (2003) 995–1017, https://doi.org/10.1137/S1064827502402120, arXiv:https://doi.org/10.1137/S1064827502402120.
[42] F. Coquel, K. El Amine, E. Godlewski, B. Perthame, P. Rascle, A numerical method using upwind schemes for the resolution of two-phase flows, J. Comput. Phys. 136 (2) (1997) 272–288, https://doi.org/10.1006/jcph.1997.5730, https://www.sciencedirect.com/science/article/pii/S0021999197957302.
[43] A. Ambroso, C. Chalons, P.-A. Raviart, A Godunov-type method for the seven-equation model of compressible two-phase flow, Comput. Fluids 54 (2012) 67–91, https://doi.org/10.1016/j.compfluid.2011.10.004, https://www.sciencedirect.com/science/article/pii/S0045793011003033.
[44] I. Toumi, A. Kumbaro, An approximate linearized Riemann solver for a two-fluid model, J. Comput. Phys. 124 (2) (1996) 286–300, https://doi.org/10.1006/jcph.1996.0060, https://www.sciencedirect.com/science/article/pii/S0021999196900601.
[45] V. Ransom, Numerical benchmark test no. 2.1: faucet flow, Multiph. Sci. Technol. 3 (1–4) (1987) 465–467.
[46] Benjamin Braconnier, Jeu-Jiun Hu, Yang-Yao Niu, Boniface Nkonga, Keh-Ming Shyue, Numerical simulations of low Mach compressible two-phase flows: preliminary assessment of some basic solution techniques, ESAIM Proc. 28 (2009) 117–134, https://doi.org/10.1051/proc/2009042.